# Noncollinear Fe spin structure in (Sm-Co)/Fe exchange-spring bilayers: Layer-resolved ^{57}Fe Mössbauer spectroscopy and electronic structure calculations

V. M. Uzdin, A. Vega, A. Khrenov, W. Keune, V. E. Kuncser, J. S. Jiang, and S. D. Bader

Phys. Rev. B **85**, 024409 — Published 11 January 2012

DOI: 10.1103/PhysRevB.85.024409

# The non-collinear Fe spin structure in (Sm-Co)/Fe exchange-spring bilayers: layer-resolved $^{57}$Fe Mössbauer spectroscopy and electronic structure calculations

V.M. Uzdin[1,2], A.Vega[3], A. Khrenov[4,a], W. Keune[4,5], V. E. Kuncser[6], J. S. Jiang[7], and S. D. Bader[7]

[1]*Department of Physics, St. Petersburg State University, St. Petersburg, 199178, Russia*

[2] *St. Petersburg State University of Information Technologies, Mechanics and Optics , St. Petersburg, 197101, Russia*

[3]*Departamento de Física Teórica, Atómica y Óptica, Universidad de Valladolid, E-47005 Valladolid, Spain*

[4]*Fakultät für Physik, Universität Duisburg-Essen, D-47048 Duisburg, Germany*

[5]*Max-Planck-Institut für Mikrostrukturphysik, D-06120 Halle, Germany*

[6]*National Institute of Materials Physics, RO-77125 Bucharest-Magurele, Romania*

[7]*Materials Science Division, Argonne National Laboratory, Argonne, Illinois 60439, USA*

## Abstract

Magnetization reversal in nanoscale (Sm-Co)/Fe (hard/soft) bilayer exchange-spring magnets with in-plane uniaxial magnetic anisotropy was investigated by magnetometry, conversion-electron Mössbauer spectroscopy (CEMS) and atomistic Fe spin-structure calculations. Magnetization loops along the easy direction exhibit signatures typical of exchange-spring magnets. In-field CEMS at inclined γ-ray incidence onto thin (2-nm) $^{57}$Fe probe layers embedded at various depths in the 20-nm thick natural (soft) Fe layer provides depth-dependent information (via the line-intensity ratio $R_{23}$ as a function of the applied field H) about the in-plane rotation of Fe spins. A minimum in the $R_{23}$–*vs*.–H dependence at ($H_{min}$, $R_{min}$) determines the field where Fe magnetic moments roughly adopt an average perpendicular orientation during their reversal from positive to negative easy axis orientation. A monotonic decrease of $H_{min}$ with distance from the hard/soft interface is observed. Rotation of Fe spins takes place even in the interface region in applied fields far below the field of irreversible switching, $H_{irr}$, of the hard phase. Formation of an Fe-Co alloy is detected in the interface region. For comparison, the non-collinear Fe spin structure during reversal and the resulting $R_{23}$ ratio were obtained by electronic structure calculations based on a quantum-mechanical Hamiltonian for itinerant

electrons. The coupling at the hard/soft interface is described by the uniaxial exchange-anisotropy field, $h_{int}$, as a parameter. Our calculated $R_{23}$ ratios as a function of the (reduced) applied field, h, exhibit similar features as observed in the experiment, in particular a minimum at ($h_{min}$, $R_{min}$). $R_{min}$ is found to increase with $h_{int}$, thus providing a measure of the interface coupling. Evidence is provided for the existence of fluctuations of the interface coupling. The calculations also show that the Fe-spin spiral formed during reversal is highly inhomogeneous. In general, our simulation of the Fe spin structure is applicable for the interpretation of experimental results on layered exchange-spring magnets.

**PACS numbers:** 75.70.-i, 75.75.-c, 71.15.-m, 76.80.+y, 75.60.Jk
Corresponding author: V. M. Uzdin, e-mail v_uzdin@mail.ru

## I. INTRODUCTION

The development of non-collinear spiral magnetic structures governed by an external magnetic field is a general phenomenon of relevance for applications in nanoelectronics and spintronics. Domain wall motion induced by current in nanowires [1], shifting of the hysteresis loop in exchange bias systems [2], domain wall magnetoresistance [3] and other phenomena are connected with the evolution of spiral spin structures under the action of applied external magnetic fields or internal fields. One of the model systems where the spiral magnetic structure can be created, controlled and reversibly tuned by an external field is the exchange spring magnet. This magnetic nanostructure, consisting of exchange-coupled hard and soft magnetic bilayers or multilayers, is an ideal system for studying how to manipulate and control non-collinear magnetic structures at the nanoscale [4].

Although experimental methods such as polarized neutron reflectometry [5] and nuclear resonant x-ray scattering [6-8], magneto-optical imaging technique [9] have been used for the investigation of the magnetization reversal process in exchange-spring and exchange-bias magnets, the determination of their magnetic structure at the nanoscale still stands as a challenging problem. A direct way to achieve such resolution in the magnetic characterization is to carry out experiments with ultrathin probe layers, which can give information about the magnetic configuration in particular atomic layers, where the probe atoms are placed. Hellwig *et al.* [10], for Fe-Pt/Ni-Fe exchange-spring films, used Co layers as a local probe of the magnetization reversal process. The Co layers, deposited either at the interface or at the top of the NiFe film, were analyzed using the soft-x-ray magneto-optical Kerr effect at the Co *L*-edge resonance. Kuncser *et al.* [11] and Keune *et al.* [12] utilized conversion electron Mössbauer spectroscopy (CEMS), incorporating the $^{57}$Fe probe layer technique, to reveal the spin structure in layered Sm–Co/Fe exchange spring systems.

One should realize, however, that the interpretation of experimental results from probe layers and, therefore, the conclusions about the magnetization reversal at the atomic scale, drawn from this interpretation, strongly depend on the underlying theoretical models. These models can be oversimplified from two viewpoints. First, for thin probe layers it is important to take into account the possibility of intermixing during the film growth which leads to the diffusion of probe atoms along the growth direction [13]. Then, instead of an ideal probe layer, we have an asymmetrical distribution of interdiffused probe-layer atoms located in a larger volume. Second, the description of the experiments is often based on a simple intuitive picture which needs to be proven to give accurate conclusions and to have a predictive character. In Ref. 10, for instance, it was assumed that the magnetic response of Co at the FePt/NiFe interface was the same as the response of the FePt interface layer because the Co layer thickness (2 nm) was taken to be significantly small as compared to the exchange length of Co (5 nm). Here, however, the influence of the upper FeNi layer on the magnetic properties of the Co slab was not taken into account. Another example is found in Refs. 11 and 12, where the authors used a

uniform spin spiral model which presupposed a linear dependence of the (in-plane) spin orientation angle in an elementary layer upon the layer depth. Such assumptions have to be confirmed on the basis of microscopic quantum-mechanical models that are able to connect the calculated magnetic configuration with the experimental data. A theory of this kind, based on non-collinear magnetic and electronic structure calculations, in which a tight-binding Hamiltonian for itinerant electrons is solved in the presence of an external magnetic field, has been recently proposed [14,15]. This theoretical approach has been shown to be reliable and suitable for describing the behavior of soft magnetic films in exchange spring magnets under external magnetic fields of different intensities and/or orientations. In particular, it enabled the calculation of the dependence of the magnetization reversal process on the thickness of the soft magnetic film, the influence of the electronic structure of cap-layers on the magnetic properties, and the jump-like transitions associated with the change of chirality of the magnetic spring in rotating applied fields. In this theoretical approach [14,15], the direction of the magnetic moment of the interfacial layer of the soft film was kept fixed along the easy axis of the hard magnet , as a first approximation, to account for both the huge uniaxial anisotropy of the hard magnet and the strong exchange interaction at the interface. Within this approximation, the reversal part of the hysteresis loop was well described, but the theory did not describe the magnetization reversal process in the whole range of the field intensities, that is, including also those high field values at which the irreversible switching of the magnetic moment of the hard magnet occurs. Here, we have extended the theoretical model by releasing this magnetic constraint at the interface.

In the present work, we have conducted CEMS measurements in external magnetic fields on Sm–Co/Fe bilayer samples with thin $^{57}$Fe probe layers placed at different distances from the Sm-Co/Fe interface to obtain site-selective (isotope-selective) data during the magnetization reversal process. We then applied our generalized theoretical model to describe, via electronic structure calculations, the experimental data at the quantum-mechanical level. We obtain an atomistic description of the non-collinear Fe spin structure in the magnetically soft Fe layer.

## II. EXPERIMENTAL AND METHODOLOGICAL PROCEDURES

Five magnetically hard (Sm-Co)/ soft (Fe) exchange spring bilayer samples with in-plane uniaxial magnetic anisotropy were prepared under the same experimental conditions using *dc* magnetron sputtering, as described in detail in Refs. 16 and 17. 20-nm thick epitaxial Sm-Co layers with a nominal $Sm_2Co_7$ composition were grown at 600°C on MgO(110) substrates with an epitaxial Cr(211) buffer layer. The epitaxial relationship for the magnetically hard Sm-Co(1 -1 0 0) layer is Sm-

Co[0001]//Cr[0 1 -1]//MgO[001]. Accordingly, an uniaxial in-plane spin structure is formed for the hard magnetic phase, with the magnetic easy axis parallel to the hexagonal Sm-Co *c* axis. In all samples the polycrystalline *bcc* iron layers, which followed the Sm-Co deposition, had a total thickness of 20 nm and were grown by sputtering at a substrate temperature $T_S$ = 300 – 400 °C. The iron layers were coated by 5 nm of Ag followed by 5 nm of Cr for protection against oxidation. Within every Fe layer, a 2-nm thick isotopically enriched $^{57}$Fe probe layer (enriched to 95% in the Mössbauer isotope $^{57}$Fe) was placed by sputter-deposition at different distances from the (Sm-Co)/Fe interface. Five samples (labeled sample A – E) were prepared, with the following composition of the hard/soft layers:

Sample A: Sm-Co(20nm)/$^{57}$Fe(2nm)/Fe(18nm)
Sample B: Sm-Co(20nm)/Fe(3nm)/$^{57}$Fe(2nm)/Fe(15nm)
Sample C: Sm-Co(20nm)/Fe(7nm)/$^{57}$Fe(2nm)/Fe(11nm)
Sample D: Sm-Co(20nm)/Fe(12nm)/$^{57}$Fe(2nm)/Fe(6nm)
Sample E: Sm-Co(20nm)/Fe(18nm)/$^{57}$Fe(2nm)

The samples are distinct only with respect to the distance of the center of the 2-nm thick $^{57}$Fe probe layer from the Sm-Co interface. These distances are 1 nm (sample A), 4 nm (sample B), 8 nm (sample C), 13 nm (sample D), and 19 nm (sample E). In sample A, the $^{57}$Fe probe layer is in direct contact with the magnetically hard Sm-Co layer. The $^{57}$Fe probe layer has the largest distance from the Sm-Co/Fe interface in sample E, where it forms the top layer on the Fe film and is in contact with the Ag cap layer. Except for the $^{57}$Fe probe layers, Fe of natural isotopic composition was used, with only 2.14% $^{57}$Fe isotopic abundance. Therefore, the Mössbauer signal of all samples originates predominantly from the $^{57}$Fe(2 nm) probe layer. If, for simplicity, we neglect the weak attenuation of the 7.3-keV conversion electrons in the Fe layer, we expect a relative Mössbauer signal of about 83% from the $^{57}$Fe probe layer and about 17% from the natural 18-nm thick Fe layer in a sample. We mention, however, that we did take the weak attenuation of the electrons into account in our theoretical model (Sec. IV).

The macroscopic magnetic properties of the samples were measured at room temperature (RT) by means of an alternating gradient magnetometer (AGM). The in-plane applied field was parallel to the easy axis direction of the magnetically hard Sm-Co layer. The spin configuration in the $^{57}$Fe probe layers during the magnetization reversal process was studied at RT by $^{57}$Fe CEMS in decreasing magnetic fields, ranging from + 1150 mT (start) to – 1150 mT (end), also applied in the film plane (xy plane) along the easy axis direction of the Sm-Co layer (y axis in Fig. 1), *i.e.*, under similar conditions

as in the AGM measurements. For detection of the conversion electrons, each sample was mounted inside of a small home-made He – 4% $CH_4$ proportional counter. The counter was placed between the poles of an electromagnet, providing the field in the sample plane. The magnetic field was continuously measured by means of a Hall probe. We noticed a substantial reduction of the count-rate in the highest fields due to the curvature of the path of the escaping electrons in the detector. A Mössbauer drive system operating in sinusoidal velocity mode combined with conventional electronics and a $^{57}$Co(Rh) source of ~ 50 mCi activity were employed. The CEM spectra were least-squares fitted using the program *NORMOS* by R.A. Brand [18].

It is known that in certain cases [19] a difference in the measurement time scale can lead to a difference in the observed values of the irreversible switching field, Hirr, of the hard magnetic layer during magnetization reversal ("magnetic after-effect" or "magnetic viscosity"). For the Mössbauer measurements, it took about 24 hours per spectrum, whereas it took about one second per data point in the AGM measurements. Thus, the time-scale of CEMS is much longer than that of AGM, and magnetic after-effects on Hirr should have saturated after such a long "aging time" of ~24 hours during CEMS, i.e., the magnetic system has achieved its ground state. During the time a CEM spectrum is taken, oscillations in the magnetic field of our Bruker electromagnet are expected to have a negligible effect on Hirr due to the very good electronic stabilization of the power supply. We have performed independent measurements of CEM spectra (not shown) with the same external field setting, and we obtained very good reproducibility of the CEMS results. As to the magnetization measurements, the AGM uses an additional pair of coils to produce an oscillating gradient in the magnetic field in order to "shake" the magnetic sample mounted on a stiff quartz rod. So the applied field which the sample experiences is not static, but has an AC component (a few kHz in frequency, and a few Oe in field amplitude). Therefore, there is an accelerated "magnetic aging" in the AGM measurement process, and it is expected that AGM and CEMS will provide similar $H_{irr}$ values.

For the investigation of the Fe spin structure by Mössbauer spectroscopy, the intensity ratio between the second (or fifth) and the third (or fourth) line, $R_{23} = I_2 / I_3 = I_5 / I_4$ , of the Zeeman-split Mössbauer sextet is the crucial experimental parameter [20]. If the direction of the hyperfine magnetic field at the $^{57}$Fe nucleus, $H_{hf}$, (which is antiparallel to the direction of the Fe atomic magnetic moment, $\mu_{Fe}$) forms an angle $\Psi$ with the incident Mössbauer $\gamma$-ray direction (Fig. 1), then $R_{23}$ is given by [20]

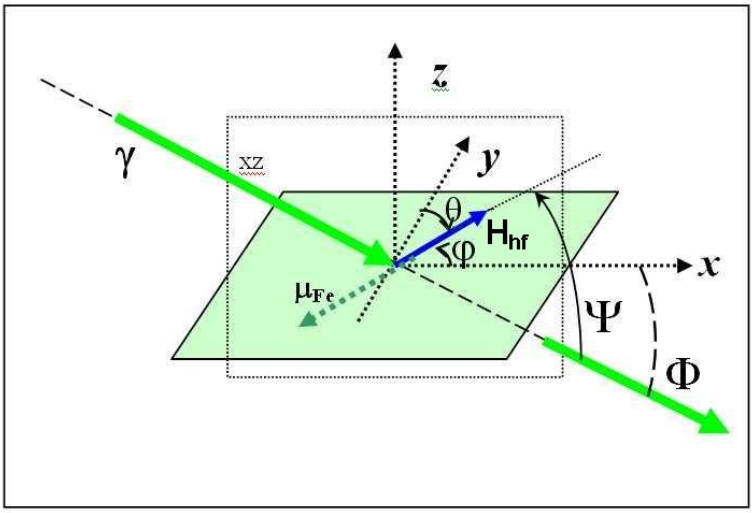


Figure 1 : Schematic geometrical arrangement of the CEMS measurement at inclined incidence of the γ-ray relative to the sample plane (xy plane). The angle of incidence Φ = 30°. The magnetic field H is applied along the Sm-Co easy-axis direction (the y axis). The hyperfine magnetic field, $H_{hf}$, (antiparallel to the Fe atomic magnetic moment, $\mu_{Fe}$) lies in the sample plane. (Ψ = angle between the γ-ray direction and the direction of $H_{hf}$). The x axis is defined by the projection of the γ-ray direction onto the sample plane.

$$R_{23} = 4\frac{<\sin^2\Psi>}{1+<\cos^2\Psi>} \quad , \qquad (1)$$

where the brackets <…> indicate averaging over the angular Fe spin distribution. For the case of strictly in-plane distributed Fe magnetic moments and the incident γ-radiation perpendicular to the sample plane, *i.e.*, Ψ = Φ = 90° in Fig. 1, the intensity ratio $R_{23}$ = 4 and is insensitive to the in-plane spin direction. Therefore, the in-plane spin configuration in our samples can be studied only in a non-perpendicular (inclined) geometry, with the γ-radiation incident at an angle Φ ≠ 90° relative to the film plane (Fig. 1). In our present experiments we have chosen Φ = 30° ± 5° as the angle of incidence. If the Fe spin directions are arranged in the sample plane with a certain angular distribution, P(φ), (with φ being the azimuthal angle relative to the x axis, Fig. 1), the intensity ratio may be expressed by the relation [20]

$$R_{23} = 4\cdot\frac{1-<\cos^2\Psi>}{1+<\cos^2\Psi>} = 4\cdot\frac{1-\cos^2\Phi<\cos^2\varphi>}{1+\cos^2\Phi<\cos^2\varphi>} \quad , \qquad (2)$$

where the brackets <…> indicate averaging over all angles φ. Due to the cos-square function, Fe spin directions at in-plane angles +φ and –φ cannot be distinguished by a measurement of $R_{23}$. From Eq. (2), the model-independent average quantity

$$< \cos^2 \Psi >= \frac{4 - R_{23}}{4 + R_{23}} \qquad (3)$$

that characterizes the angular distribution of the Fe spins can be obtained from a measurement of the Mössbauer line-intensity ratio $R_{23}$.

Often experimental values of $R_{23}$ are compared with theoretical $R_{23}$ ratios simulated on the basis of reasonable model distributions P(φ) [11,20]. The simplest model implies the unidirectional distribution P(φ) with a unique Fe spin direction. It was applied to describe the Fe spin structure in Fe/$MnF_2$ exchange-biased bilayers [8, 21]. A more realistic model uses a step-shaped planar distribution P(φ), where the in-plane spins are assumed to be located in a certain angular interval and show homogeneous fanning. This model was employed to deduce the Fe spin structure in Fe/$MnF_2$ exchange-biased bilayers [21] and in (Sm-Co)/Fe bilayer spring magnets [11]. However, in the present work we do not need to use a specific model for the distribution P(φ). We compare our experimental $R_{23}$ ratios with theoretical $R_{23}$ values obtained from the atomistic spin structure calculations in Sec. IV. This comparison provides model-independent information on the layer resolved in-plane Fe spin structure in our samples.

## III. EXPERIMENTAL RESULTS

### A. Magnetization

The RT magnetic hysteresis loops along the easy-axis direction of our five Sm-Co(20nm)/Fe(20nm) bilayers are shown in Fig. 2. This measurement provides a macroscopic average for the magnetic reversal process of each sample. The loop shapes observed in Fig. 2 display a double step and are typical for layered exchange-spring magnetic systems [19,22-24]. Upon decreasing the field from positive saturation, a sharp drop of the magnetization occurs at the so-called nucleation field $\mu_0 H_n$ (also called exchange field $\mu_0 H_{ex}$ in Ref. 22) just below $\mu_0 H$ = 0 T, followed by a signature of saturation around $\mu_0 H$ = 350 mT. Separate switching transitions are observed for the Fe and Sm-Co layers. The nucleation field $H_n$ in the low-field range reflects the reversible magnetization reversal of the soft Fe layer, whereas the switching field $H_{irr}$ in the high-field region is indicative for the irreversible switching of the hard Sm-Co layer. As expected, the loop shape is similar for all five samples in the low- and medium-field range, since chemically the Fe layers have the same total

thickness of 20 nm in all samples. In fact, the measured nucleation field $\mu_0 H_n$ is about the same for all samples (~ 100 mT in absolute value), in good agreement with the value of ~ 90 mT reported in the literature [22]. Further, the coercive field, $\mu_0 H_C$, of ~310 mT is about the same for all five samples. However, although the samples were grown under the same conditions, there is a spread of $H_{irr}$ values observable, as can be seen more clearly in the insert of Fig. 2. This means that less controllable variations of the sample properties during their preparation (*e.g.*, changes in the exchange coupling between the hard and soft layer due to interdiffusion and /or changes in the local magnetic anisotropy due to compositional variations at the hard / soft interface caused by interdiffusion [17]) affect the switching of the Sm-Co layer.

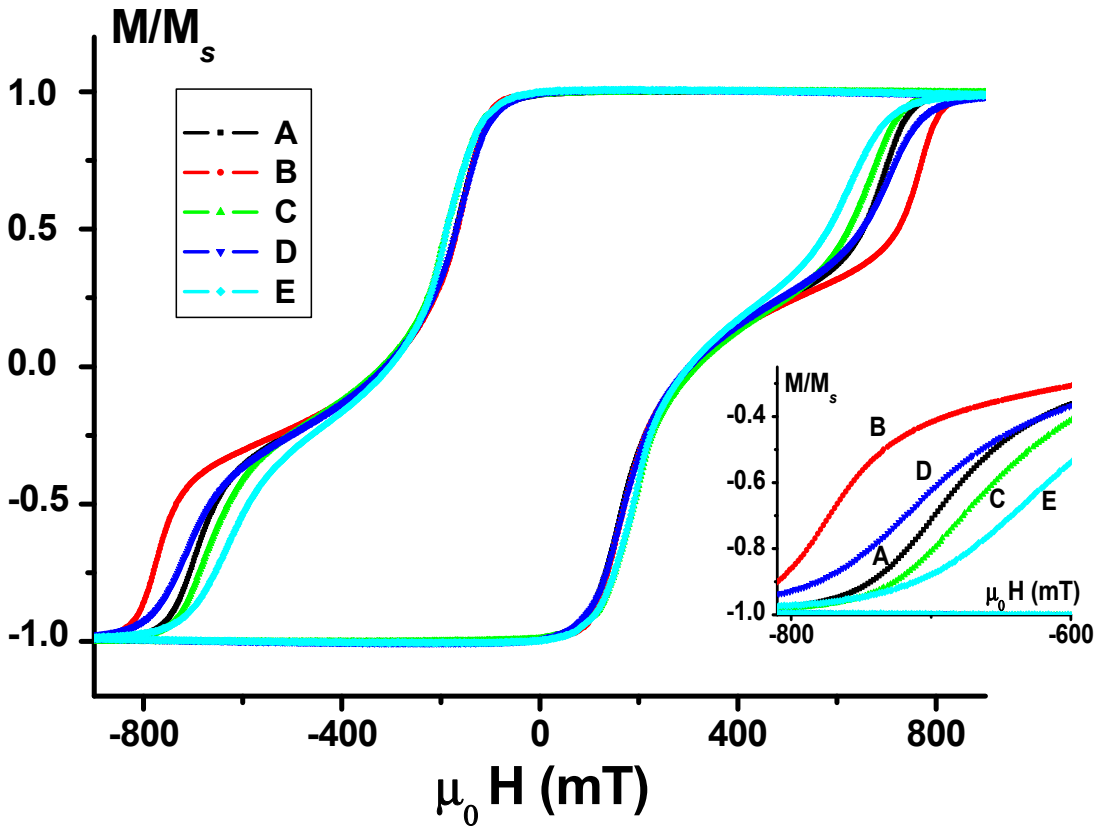


Figure 2: RT magnetic hysteresis loops for Sm-Co(20nm)/Fe(20nm) bilayer films (samples A – E) with the magnetic field H applied parallel to the easy axis direction. The magnetization M is normalized by the saturation magnetization $M_s$. The inset shows the enlarged left region of the loop.

If we define $H_{irr}$ as the magnetic field at the intersection of the two tangent lines going through the two inflection points in the (negative) high-field region, then we can estimate $\mu_0 H_{irr}$ values of -650, -730, -590, -640 and -540 mT for samples A, B, C, D and E, respectively, *i.e.*, the observed $\mu_0 H_{irr}$

values range between ~ -540 and -730 mT. Furthermore, we can define the field $H_S$ , for which the reverse saturation for the whole bilayer is approximately achieved, as the intersection of the tangent line at the inflection point of the highest (negative) field region with the field axis. This provides $\mu_0 H_S$ values of -750, -820, -740, -790 and -715 mT for samples A, B, C, D and E, respectively. Thus, saturation is approximately achieved in the field range between ~ -715 and -820 mT. In Sec. III.B we will compare $H_{irr}$ and $H_S$ with corresponding values obtained from the layer-resolved $R_{23}$ – *vs*. – H behavior via Mössbauer spectroscopy.

**B. Mössbauer spectroscopy**

Typical RT CEM spectra taken under an angle of incidence of $\Phi = 30°$ and in different applied fields are presented in Fig. 3 (a) and (b) for sample E and D, respectively, and in Fig. 4 (a) and (b) for sample B and A, respectively. The spectra of sample C (not shown) are of similar quality. The spectra were measured in the sequence from the highest (positive) field to the lowest (negative) field, as indicated in Figs. 3 and 4. All spectra of samples B, C and D (which have $^{57}$Fe probe layers in the inner part of the iron film) are seen to be simple Zeeman sextets typical for α-Fe, as expected for the 2-nm-thick $^{57}$Fe probe layers embedded by (natural) α-Fe layers on both sides. These spectra were least-squares fitted with one sextet with Lorentzian lines and a narrow linewidth (full width at half maximum) of ~ 0.34 mm/s. The hyperfine magnetic field, $H_{hf}$, obtained from this fitting is $\mu_0 H_{hf}$ = 32.7(1) T, which is in good agreement with the value of 33.0 T of bulk α-Fe at RT [25]. Together with the observed negligible electric quadrupole interaction and the negligible isomer shift (relative to bulk α-Fe at RT) this observation proves that the inner part of our Fe films consist of the α-Fe phase.

On the other hand, for the fitting of the spectra of sample E (surface) a very weak subspectrum with a hyperfine field distribution $P(H_{hf})$ and with a relative spectral area (relative integrated spectral intensity) of only 4 – 6 % had to be added as a small correction to the dominant sharp α-Fe sextet (with a high spectral area of 96 – 94 %) in order to take into account the weak line asymmetries on the inner sides near the foot of the sextet lines. This distribution $P(H_{hf})$ (not shown), which made a weak but non-negligible contribution in the $\mu_0 H_{hf}$ range between ~ 25 - 29 T, is attributed to a small fraction of $^{57}$Fe-probe layer atoms sensing atoms of the polycrystalline Ag overlayer in sample E. This $H_{hf}$ range coincides reasonably well with the range of hyperfine fields (28.7 – 30 T) observed by Schurer *et al.* [26] for a 1.4-ML-thick $^{57}$Fe probe layer at the Ag(001) interface at RT. The spectral area of 94 - 96 % indicates that effectively ~1.9 nm of the 2-nm thick $^{57}$Fe probe layer corresponds to bcc Fe, whereas the spectral area of 4 – 6 % shows that a thickness of effectively ~ 0.1 nm (or about one Fe

atomic layer) of the $^{57}$Fe probe-layer atoms sense Ag atoms at the Ag/Fe interface. This provides evidence of negligible interdiffusion at the Ag/Fe interface.

The spectra of sample A [Fig. 4 (b)], in which the $^{57}$Fe probe layer is in contact with the Sm-Co layer, are sextets with broad and asymmetric lines. In particular, shoulders are observable on the outer sides of the outer sextet lines. In agreement with our earlier work [11] these spectra could be fitted only by two sextets with sharp Lorentzian lines as spectral components. At zero external field, the dominant sextet (with a relative spectral area of 65.3 %) has $\mu_0 H_{hf}$ = 32.7(1) T, a nearly negligible isomer shift $\delta$ of – 0.009(3) mm/s (relative to bulk α-Fe at RT) and a negligible electric quadrupole interaction. This proves that about 65 % of the $^{57}$Fe probe atoms are forming the α-Fe phase. For the second sextet (satellite spectrum of 34.7 % in relative spectral area), at zero external field, the fitting provided a hyperfine field $H_{hf}$ of $\mu_0 H_{hf}$ = 34.2(1) T, a very small positive isomer shift of $\delta$ = 0.035(5) mm/s (relative to bulk α-Fe at RT) and negligible quadrupole interaction. By correlating the measured relative spectral areas of the two sextets of sample A (65.3 % and 34.7 %, respectively) with the corresponding hyperfine field values (32.7 T and 34.2 T, respectively), we conclude that the outer sextet with the enhanced $\mu_0 H_{hf}$ value of 34.2(1) T originates from an interfacial Fe-rich *bcc* Fe-Co alloy formed by interdiffusion into an effectively about 0.7-nm-thick $^{57}$Fe region in the probe layer at the (Sm-Co)/$^{57}$Fe interface, whereas the rest (effectively about 1.3 nm ) of the 2-nm-thick $^{57}$Fe probe layer exists in the pure α-Fe phase. This conclusion is based on the fact that Co impurities in *bcc* Fe enhance the hyperfine field [27], by analogy with the magnetic moment enhancement by Co impurities in *bcc* Fe that follows the Slater-Pauling curve [28]. Since the satellite spectrum of sample A is typical for an Fe-Co alloy and not for an Fe-Sm alloy or compound, we conclude that the interfacial Fe-Co alloy is mainly formed by outdiffusion of Co atoms from the Sm-Co layer into the interfacial $^{57}$Fe probe layer, very likely during sample preparation. Obviously, $^{57}$Fe CEMS is a powerful method for the analysis of phase formation at the buried Sm-Co/Fe interface.

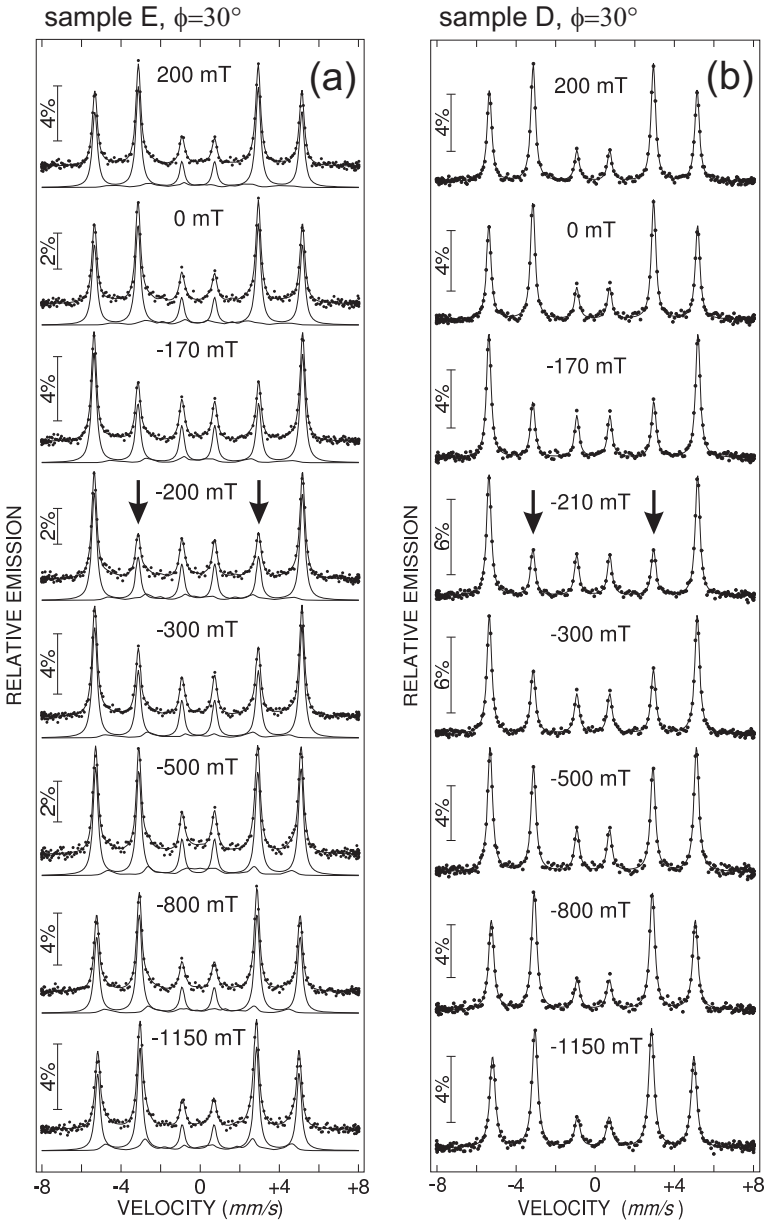


Figure 3: RT CEM spectra of (a) sample E (surface) and (b) sample D, taken at inclined incidence of the γ-radiation (Φ = 30°) and in different magnetic fields applied along the easy axis direction in the film plane (along the y direction). For each sample, the sequence of measurements started with the highest (positive) field and finished with the lowest (negative) field. The least-squares fitted curves are described in the text.

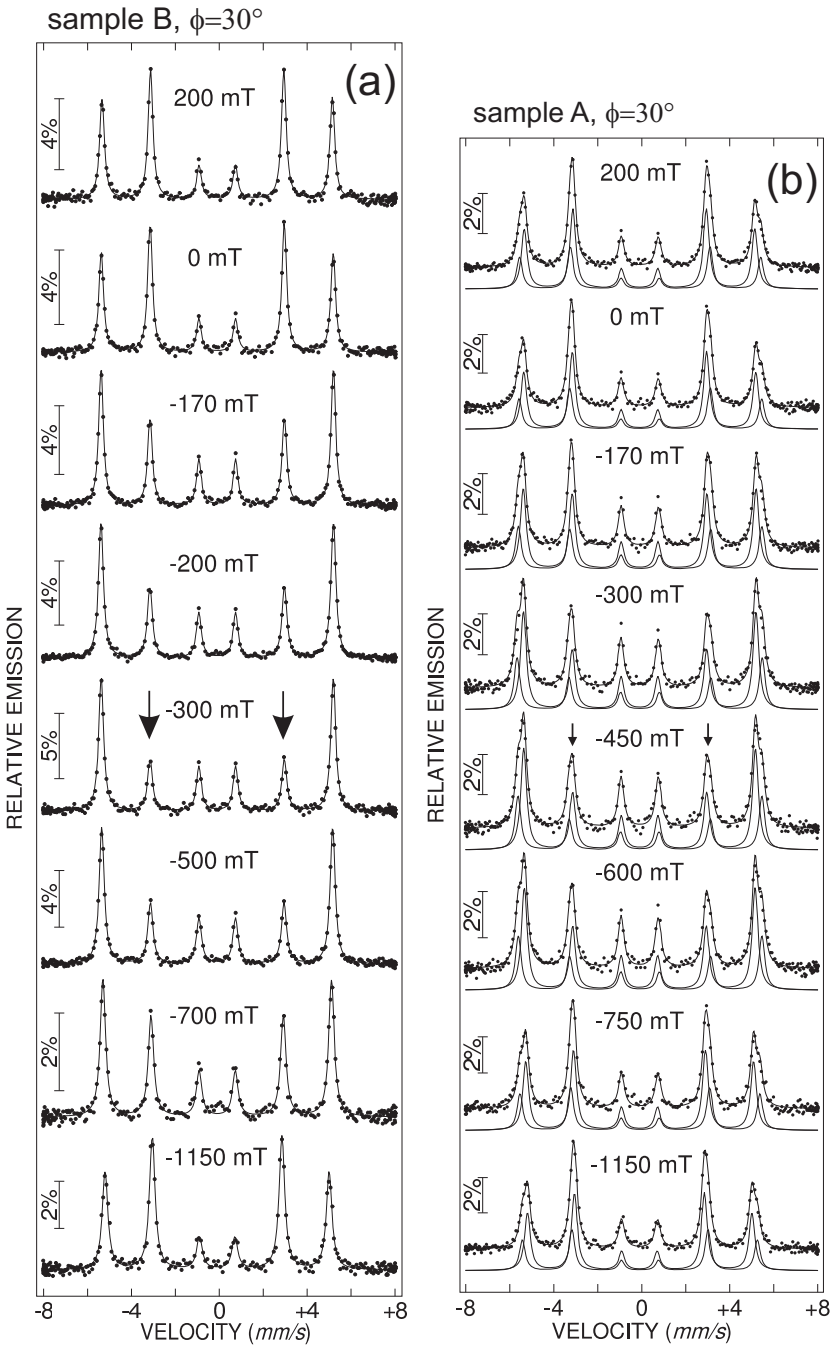


Figure 4: RT CEM spectra of (a) sample B and (b) sample A (interface), taken at inclined incidence of the γ-radiation (Φ = 30°) and in different magnetic fields applied along the easy axis direction in the film plane (along the y direction). For each sample, the sequence of the measurements started with the highest (positive) field and finished with the lowest (negative) field. The least-squares fitted curves are described in the text.

The striking effect observed in the CEM spectra of Figs. 3 and 4 is the systematic variation of the relative intensity of lines # 2 and 5 (marked by vertical arrows) as a function of the applied field H.

For all samples, at applied fields $\mu_0 H \geq \sim +$ 200 mT, the line intensity ratio of the sextet is measured to be about 3 : 4 : 1 : 1 : 4 : 3, i.e., $R_{23} = 4$, as expected from Eq. (1) for full alignment of the Fe magnetic moments along the + y direction (Fig. 1) and for an angle $\Psi = 90°$ between the $\gamma$-ray direction and the y axis. $R_{23} = 4$ is also measured for the largest negative fields (at $\mu_0 H = -$ 1150 mT), *i.e.*, for full magnetic alignment along the – y direction. For intermediate (decreasing) applied fields, the relative intensity of the lines # 2 and 5 (or the $R_{23}$ ratio) changes drastically and systematically. Minimum $R_{23}$ values are observed at applied fields $\mu_0 H_{min}$ of – 200 mT for sample E (surface), - 210 mT for sample D, - 300 mT for sample C (not shown), - 350 mT for sample B, and - 450 mT for sample A (interface). The observed variation of the relative intensities of lines # 2 and 5 is an atomistic manifestation of the Fe spin reversal process, essentially layer-resolved on a nanoscale.

The measured dependence of the line intensity ratio $R_{23}$ upon the in-plane external field $\mu_0 H$ is presented in Fig. 5. With decreasing field, starting from saturation at + 1150 mT, $R_{23}$ remains approximately constant at a value near 4, until a sharp drop occurs below $\mu_0 H = 0$ T followed by the development of minimum in $R_{23}$, with a subsequent increase to a final value of 4 at the saturating field of – 1150 mT. Phenomenologically, the observed behavior of $R_{23}(H)$ resembles that of $M(H)/M_S$ in Fig. 2: the sharp drop in the low-field region occurs at the nucleation field $H_n$ followed by the reversible part of $R_{23}(H)$ and saturation at a minimum $R_{23}$ value, $R_{min}$. The steep rise in $R_{23}(H)$ for decreasing applied fields below the minimum reflects the rotation of the preferential Fe spin orientation towards the negative external field direction (y direction, Fig. 1), *i.e.*, $H = H_{min}$ determines the switching of the Fe spin structure from preferential positive to preferential negative direction. (One should remember that according to Eq.(2) in-plane angles $+\varphi$ and $-\varphi$ cannot be distinguished by a measurement of $R_{23}$). The difference between $R_{23}(H)$ and $M(H)/M_S$ is that the former quantity is layer resolved. It is observed in Fig. 5 that the smaller the distance of the $^{57}$Fe probe layer from the Sm-Co/Fe interface, the broader becomes the minimum; it is the broadest for sample A (interface) (see insert in Fig. 5). The following values are found for the $R_{23}$ minima, $R_{min}$ : 1.2(1) for sample E (surface) at $\mu_0 H_{min} = -$ 200 mT, 1.15(10) for sample D at $\mu_0 H_{min} = -$ 210 mT, 1.16(10) for sample C at $\mu_0 H_{min} =$ – 300 mT, 1.16(10) for sample B at $\mu_0 H_{min} = -$ 350 mT, and 1.7(1) for sample A (interface) at $\mu_0 H_{min} = -$ 450 mT. It is remarkable that samples B, C, D and E , in which the $^{57}$Fe probe layers are away from the Sm-Co/Fe interface, exhibit the same value of $R_{min} = 1.2(1)$ within error bars, whereas sample A (with its $^{57}$Fe probe layer directly at the interface) has a considerably higher value of $R_{min} =$ 1.7(1). When $R_{min}$ is reached, according to Eq. (2), the $^{57}$Fe spins (predominantly in the $^{57}$Fe probe layer) have acquired such a particular in-plane angular distribution $P(\varphi)$ or Fe spin texture that, in the average, they are closest to the direction of the in-plane projection of the incoming $\gamma$-ray, *i.e.*, parallel to the x axis or at $\theta = 90°$ with respect to the easy axis direction (Fig. 1). Thus, $H_{min}$ is the field where

the Fe spins roughly adopt an average perpendicular orientation during the reversal from positive to negative easy axis (y axis) orientation. If all Fe spins are uniformly (unidirectionally) oriented along the x axis (i.e., for $P(\varphi) = \delta(\varphi - \varphi_0)$ with $\varphi_0 = 0°$), a lower limit of $R_{min} = 0.57$ (or an upper limit of $\langle\cos^2\varphi\rangle_{min} = 1$) is expected from Eq.(2) for our experimental geometry ($\Phi = 30°$). Such a low $R_{min}$ value (or high $\langle\cos^2\varphi\rangle_{min}$ value) is not observed for any of our samples (according to Eq. (2), $R_{min} = 1.2$ corresponds to $\langle\cos^2\varphi\rangle_{min} = 0.72$ and $R_{min} = 1.7$ corresponds to $\langle\cos^2\varphi\rangle = 0.54$). The higher $R_{min}$ values (or lower $\langle\cos^2\varphi\rangle_{min}$ values) observed here indicate in a qualitative way that the in-plane Fe spin distributions $P(\varphi)$ in the samples include in-plane Fe spins that are canted relative to the x axis ($\theta = 90°$ or $\varphi = 0°$). This deviation is most pronounced for sample A (interface sample) with its high value of $R_{min} = 1.7$ (or $\langle\cos^2\varphi\rangle_{min} = 0.54$). On the other hand, for the other samples B – E (with their $^{57}$Fe probe layers at a distance from the interface), the common observed $R_{min}$ value of 1.2(1) implies that these samples reach similar Fe spin distributions when the applied field approaches their respective $H_{min}$ value. These observations prove in a model-independent way that upon magnetization reversal the Fe spins at the Sm-Co/Fe interface form a larger average angle $\varphi$ (or smaller average angle $\theta$) than the Fe spins more distant from the interface. This different behavior is a consequence of the strong interfacial exchange coupling. One may notice that the magnitude of $H_{min}$ increases for probe layers closer to the interface. We will show in the theoretical section that these qualitative conclusions from our experiment are supported in a quantitative way by our calculations.

In Fig. 5, we indicate the range of irreversible fields, $H_{irr}$, the range of saturation fields, $H_S$, and the coercive field, $H_C$, for samples A – E, as obtained from our magnetization measurements (Sec. III.A).The coercive field is the field at which the (macroscopically averaged) magnetization changes from positive to negative direction along the easy axis (y axis). One may notice in Fig. 5 that with decreasing negative field samples E and D (with their $^{57}$Fe probe layers far away from the interface by 19 nm and 13 nm, respectively) reach their $R_{23}$ minimum at $\mu_0 H_{min}$ before the coercive field $\mu_0 H_C$ of -310 mT is approached. This means that Fe spins in layers at 13 nm or more from the interface rotate from positive to negative y direction before $H_C$ (defined for the overall bilayer system) is reached. For samples C and B with their probe layers closer to the interface (*i.e.*, 8 and 4 nm, respectively), $H_C$ is close to or at $H_{min}$ of these samples, which means that reversal of the Fe spin direction within the distance-range of 8 nm to 4 nm occurs around $H_C$. The most interesting case is sample A with its $^{57}$Fe probe layer in direct contact with the hard Sm-Co layer: $\mu_0 H_{min}$ for sample A appears ~ 140 mT below $\mu_0 H_C$. Apparently, upon decreasing the applied field, the reversal of the Fe spin direction in the interfacial region appears far below $H_C$. This effect originates from the strong exchange coupling at the interface between the hard Sm-Co layer and the Fe layer. Thus, the Fe interface layer, in proximity

with the hard Sm-Co layer, responds like a semi-hard magnet. Note, however, that Fe spin rotation in this interfacial region starts already for small negative fields.

As indicated in Fig. 5, the range of irreversible fields, $H_{irr}$, as obtained from the hysteresis loops in Fig. 2, coincides reasonably well with the strong rise of $R_{23}$ with decreasing applied field below the $R_{23}$ minimum of the different samples. This steep rise of $R_{23}$ reflects (in a layer-resolved way) the irreversible magnetization reversal of the hard Sm-Co layer and the Fe layer. The range of negative saturation fields, $H_S$, as deduced from Fig. 2 for the different samples, agrees well with the field range in Fig. 5, where the $R_{23}$ ratio approaches the value of 4, indicating complete Fe spin alignment along the negative field (and negative y) direction.

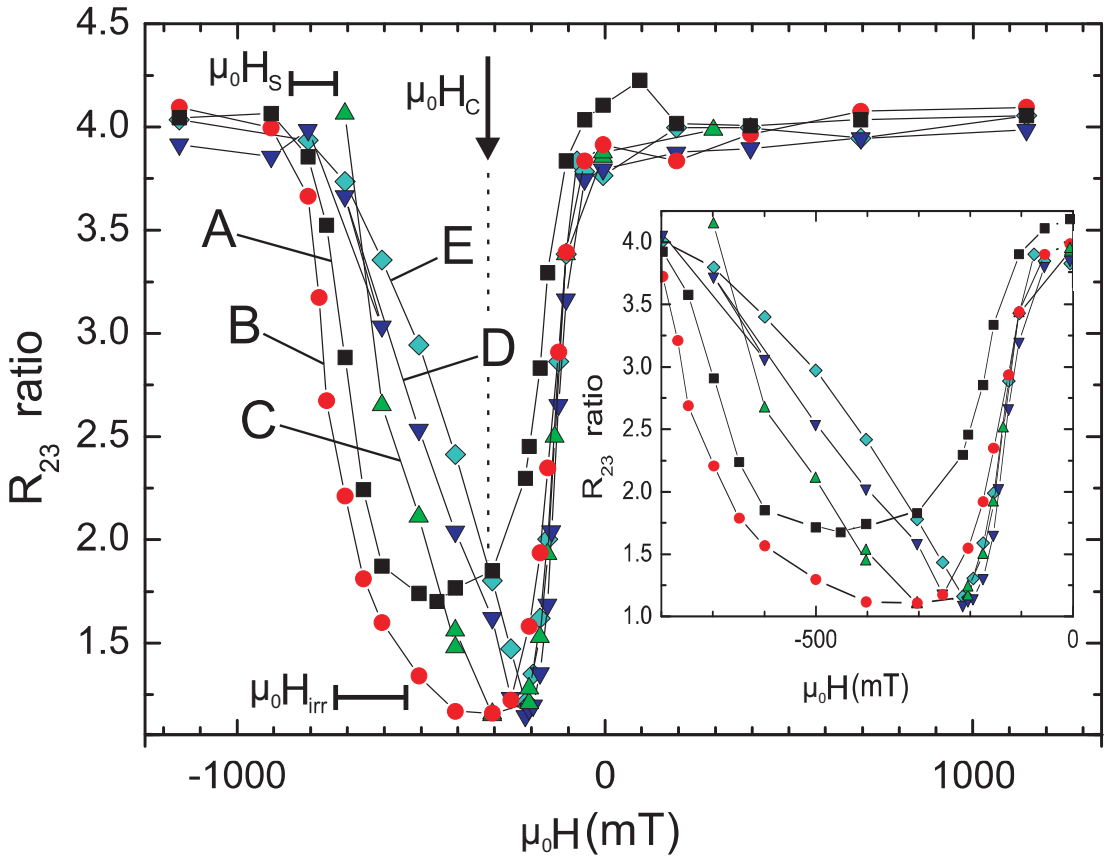


Figure 5: Experimental Mössbauer line-intensity ratio $R_{23}$ versus the external field $\mu_0 H$ applied along the easy axis direction and following the decreasing field branch of the hysteresis loop, obtained from least-squares fitting the CEM spectra of samples A – E. Black squares: sample A (interface); red

circles: sample B; green triangles tip up: sample C; dark-blue triangles tip down: sample D; light-blue diamonds: sample E (surface). (The lines are a guide for the eye). The range of irreversible fields, $H_{irr}$ , the range of saturation fields, $H_S$ , and the coercive field, $H_C$ , for the five samples measured by magnetometry are also indicated.

## IV. THEORETICAL MODEL

For the theoretical description of the magnetization reversal process of the Fe layers as soft component of the spring magnet, we have performed electronic structure calculations in the framework of a non-collinear tight-binding model [14,15]. We assume the existence of two bands, one associated with the quasilocalized but itinerant *d* electrons, responsible for magnetism, whereas the other band describes the delocalized *sp* electrons. On-site Coulomb repulsion has been taken into account in the unrestricted Hartree-Fock approximation. To describe non-collinear magnetic configurations, the Hartree-Fock approximation was performed in the local reference system of each atom with the quantization axis along the local magnetic moment. After moving to the laboratory reference system, with unique quantization axis for the whole magnetic moments in the system, the equations for *d*-electron Greens functions contain additional on-site hopping with spin flip due to the change of the spin basis at each atomic site. This hopping is proportional to the projection of the local moment onto the plane perpendicular to the quantization axis. We note that there are no new parameters in the non-collinear framework as compared with the collinear approach [14,15].

The *s-d* hybridization leads to the appearance of a finite *d*-electron level width $\Gamma$. All the energy parameters of the model are measured in units of $\Gamma$. Thus, the model contains very few semiempirical dimensionless parameters. These parameters determine the position of the *d* states relative to the Fermi level, $(E_0 - \varepsilon_F)/\Gamma$ , the on-site Coulomb repulsion, $U/\Gamma$, and the hopping integrals between nearest neighbors atoms, $V/\Gamma$. Values of these parameters were fitted in order to reproduce *ab initio* results for various ideal systems as well as experimental data obtained by complementary methods. It has been shown that the model captures the main peculiarities of the magnetic behavior of Fe in different environments. In particular, it was used for the interpretation of Mössbauer spectra in the multilayer systems Fe/Cr [13] and Fe/V [28]. For bcc Fe, we used the parameters $(E_0 - \varepsilon_F)/\Gamma = -11.5$, $U/\Gamma = 13$ and $V/\Gamma = 0.9$ [13-15,29].

For the investigation of the magnetization reversal process in the (Sm-Co)/Fe exchange spring magnet, calculations at different values of an external magnetic field have been performed. Here, the laboratory quantization axis has been chosen along the external field which was taken along the hard-layer anisotropy axis opposite to the original saturation magnetic moment of the hard magnet. In our

previous calculations [14,15], the direction of the Fe magnetic moment at the interface with the hard magnet was kept fixed to model the strong exchange coupling at the interface and the huge uniaxial anisotropy of the hard magnet. The experimental behavior of sample A with respect to the $R_{23}$ ratio (Fig. 5) shows that even the Fe spins in the probe layer in intimate contact with the Sm-Co layer rotate with the applied field. Therefore, we generalize the theoretical model by releasing the condition of infinite uniaxial anisotropy in the hard magnet. Thus, we permit rotation of the Fe interfacial layer by considering in this layer an internal magnetic field ($H_{int}$), strong but finite and oriented along the magnetic moment of the hard magnet. As is seen from experiments, the exchange coupling between the hard and soft phases strongly depends on details of the sample preparation and can be modified, for example, by annealing of the sample [30]. The possible variation in a broad range of the exchange coupling at the SmCo/Co interface was also confirmed through *ab initio* calculations [31]. We note that in those calculations, the value of the internal field was about one to two orders of magnitude larger than the external magnetic field applied to the whole sample. Note, however, that magnetization reversal of the hard magnet can start in an external field that is weaker than $H_{int}$ even for very thin soft magnetic layers. In this last case, the magnetic moments of the hard and soft phase rotate simultaneously as a whole without formation of a spiral magnetic structure. This corresponds to the 'rigid magnet' regime [24,32].

When the magnitudes and directions of the local magnetic moments, at each atomic layer, are determined, the ratio $R_{23}$ between the second and the third lines of Mössbauer spectra can be calculated for particular probe layers or for the whole sample. We consider a N atomic-layers thick Fe slab as the soft phase of the spring magnet. This Fe slab contains $^{57}$Fe atoms only in the n probe layers $i = i_0, \ldots, i_0+n-1$, counting from the interface layer. $R_{23}$ can be calculated using eq. (2) with:

$$\left\langle \cos^2 \Psi \right\rangle = \frac{\cos^2 \phi}{n < \alpha_n >} \sum_{i=i_0}^{i_0+n-1} \sin^2 \theta_i \left(1 - p_{Fe}(N-i)\right) \quad . \qquad (4)$$

Here $\phi$ is the angle between the radiation beam and the surface of the sample (or x axis in Fig. 1); $\theta_i$ = is the angle of the magnetic moment of the i-layer of Fe, taking as a reference the easy direction of the magnetization of the hard magnet. (Thus, the angle $\theta_i$ is connected with the correspondent angle $\varphi_i$ (Fig.1) by the relation $\theta_i + \varphi_i = 90°$). The bracket under the summation as well as the factor

$$< \alpha_n >= 1 - p_{Fe}\left(N - i_0 - \frac{n}{2}\right) \qquad (5)$$

take into account the weak attenuation of the conversion electron response due to the effects of scattering and absorption before escaping from the sample surface [11]. The coefficient $p_{Fe}$ describes the weakening of the electron yield per one Fe monolayer with increasing depth. For the energy-integrated conversion electron transmission versus depth z we have employed the transmission

function ("weight function") $T_t(z)$ given by Liljequist *et al.* [33], as described in Ref. 11. However, as a somewhat better approximation than in Ref. 11 for the case of small film thicknesses, which is applicable here, we have used the transmission function $T_t(z) = 1 - 0.011z$ (with z in nm). It is worth mentioning that for the small thickness of our samples, the depth dependence of the weight function, $T_t(z)$, induces only minor variations of the intensity ratio $R_{23}$ (less than 0.1), generally lower than the experimental errors.

If we consider in the sample two Mössbauer-active regions with thicknesses $n_{(1)}$, $n_{(2)}$ and concentrations of $^{57}$Fe atoms $c_{n(1)}$, $c_{n(2)}$, respectively, the resulting $R_{23}$ ratio can be obtained from the following average:

$$< \cos^2 \Psi >= \frac{n_{(1)} < \alpha_{n(1)} > c_{n(1)} < \cos^2 \Psi >_{n(1)} + n_{(2)} < \alpha_{n(2)} > c_{n(2)} < \cos^2 \Psi >_{n(2)}}{n_{(1)} < \alpha_{n(1)} > c_{n(1)} + n_{(2)} < \alpha_{n(2)} > c_{n(2)}} \quad , \quad (6)$$

where $< \cos^2 \Psi >_{n(1)}$, $< \cos^2 \Psi >_{n(2)}$, $< \alpha_{n(1)} >$, $< \alpha_{n(2)} >$ are the values calculated using Eqs. (4) and (5) for the corresponding Mössbauer active regions. In principle these regions can overlap so that for the samples studied in the experiment we can consider the entire Fe slab with thickness N to consist of the natural iron layer with $c_1=c_{nat}$ as the first region and the probe layer with $^{57}$Fe concentration $c_2= c_{probe}-c_{nat}$ as the second one. The $R_{23}$ ratio can be calculated via $< \cos^2 \Psi >$ using Eq. (2)

The standard theoretical approach for the description of the magnetization reversal process is based on the micromagnetic modeling of the system using a one-dimensional continuum model or a discrete chain model [6,9,17,22,23,32,34]. These models provide a good intuitive picture of the magnetization reversal process and are very useful for a qualitative understanding of the magnetic behavior. Such calculations require relatively little computational time but include phenomenological parameters which are fitted for the description of experimental data on the magnetization reversal process in spring-magnet systems. Contrary to micromagnetic modeling, the *intrinsic* parameters of our quantum-mechanical model are no fitting parameters for the description of the magnetic reversal mechanism in the Fe layer. They can be determined, for example, from the well-known magnetic moment and d-electron number of bulk Fe, or from comparison with *ab-initio* calculations of some ideal systems, e.g., surfaces and interfaces. There are a large number of such calculations, and the parameters of Fe within our model for Fe are well known now; and they are given above.. Using these parameters, many calculations were performed [13-15,29], and it was shown that the model that uses such parameters gives a good description of the magnetic structure of Fe atoms in different local environments. These intrinsic parameters were **fixed** for our present system. Therefore, when we calculate the Fe spin structure in external magnetic fields in the non-collinear approach, we do not introduce additional parameters for our present system. Fitting parameters can appear in the theory

only as *extrinsic* ones to describe the influence of the environment that is not included in the system, such as the exchange-anisotropy field $H_{int}$ (or $h_{int}$) at the hard/soft interface in the present case.The microscopic self-consistent calculations are time-consuming and need large computational efforts. However, the advantage of this microscopic approach is that all approximations are controlled and can be systematically improved taking into account additional microscopic interactions (e.g., spin-orbit interaction), but not via modification of *intrinsic* parameters of the model.

## V. CALCULATED Fe SPIN STRUCTURE AND MÖSSBAUER DATA

We have performed calculations for a 100-ML (monolayers) thick Fe film on the surface of a hard magnet, with a uniform external magnetic field applied opposite to the magnetization of the hard phase. This structure corresponds to the one studied experimentally in Ref 11, but with a smaller Fe thickness than in the samples studied experimentally (~ 140 ML) in this paper. (Our aim is to understand the general trends, and considering the larger thickness is more computationally demanding). Correspondingly, for comparison with the CEMS data, we proportionally reduce the thickness of the $^{57}$Fe probe layer from ~14 ML in the experiment to 10 ML in our calculations.

The exchange interaction with the hard magnet was modeled either by fixing the direction of the magnetic moment of the Fe interface, as in our previous works [14,15], or by applying a strong but finite uniaxial internal anisotropy field at this interface, as explained in the previous section. The first case corresponds to a very large internal interfacial anisotropy field that we denote as $H_{\rm int} = \infty$ below. We note, however, that this field is not large enough to change essentially the modulus of the interface moment. Within the more general second approach, two different values for $H_{int}$ have been considered. The anisotropy fields, estimated from extrapolating the hard-axis loop to saturation, are about 20 – 40 T [22]. Therefore, different values of $H_{int}$ around this estimation are considered in the calculations. In units of $\Gamma$, we have taken $h_{int} = \mu_B H_{int} / \Gamma = 3\cdot10^{-3}$ and $2\cdot10^{-3}$, which correspond to fields $H_{int}$ of the order of a few tens of Teslas [14]. More specifically, $h_{int} = 3 \times 10^{-3}$ and $2 \times 10^{-3}$ corresponds to fields $H_{int}$ of about 52 T and 35 T, respectively, assuming $\Gamma = 0.1$ eV. After the self-consistent calculations of the non-collinear spin-polarized electronic structure, the charge- and magnetic moment-distribution within the system as a function of the external magnetic field is obtained. From the magnitudes and directions of the local magnetic moments, on each Fe-site, we have calculated the average moment in the different probe regions from the interface to the surface, that is, in layers 1-10, 15-24, 35-44, 91-100 as well as in the whole sample (labeled 'all').

The results obtained for these average magnetic moments for the different values of $H_{int}$ and as a function of the external field, are depicted in Fig. 6. We plot the longitudinal ($M_y$) and transverse ($M_x$) components of the average moment, as well as its modulus |M| [with $|M| = (M_x^2 + M_y^2)^{1/2}$] and the angle θ formed with the direction of the easy axis of the hard magnet (y axis in Fig. 1). The exchange coupling at the interface decreases as going from $h_{int} = \mu_B H_{int} / \Gamma = \infty$ to $3 \cdot 10^{-3}$ and $2 \cdot 10^{-3}$. The horizontal scale unit in Fig. 6 corresponds to a field of roughly 173 mT, assuming Γ = 0.1 eV. For the surface layers (91-100) being far from the interface, all dependencies are very similar and independent of the exchange coupling with the hard magnet (see upper row in Fig. 6). However, for the interface layers (1-10) the results strongly depend on the conditions at the interface: for $H_{int} = \infty$, the longitudinal and transverse components of magnetization change little with the applied field, although the change in the modulus |M| of the Fe moment is slightly larger than for the other probe layers. The latter fact means that near the interface, the rotation of the Fe magnetic moments from one atomic layer to the next one is larger than in the upper part of the sample closer to the surface. Therefore, even in a narrow Fe slab near the interface the distribution of magnetic moment directions will be less homogeneous than in a similar slab near the surface However, as can be concluded from the field-dependence of |M|, inside of the thin 10 ML probe region the relative rotation of the magnetic moments is rather small and, when averaged, the modulus stays almost constant. This suggests that the assumption of a uniform Fe spin direction within the thin (10 ML) $^{57}$Fe probe layers during magnetization reversal, sometimes made for the analysis of CEMS data [11,12], is justified. The modulus |M| of the average magnetic moment for the whole sample monotonically decreases for $H_{\text{int}} = \infty$, but it reaches a minimum and increases again for finite values of $H_{int}$, even if they are of the order of tens of Tesla. Such behavior is connected with the rotation of the magnetic moment of the interface Fe layer together with the irreversible magnetization reversal of the hard magnet, which is prevented in the calculation if $H_{\text{int}} = \infty$.

The dependence on the external magnetic field of the longitudinal ($M_y$) and transverse ($M_x$) components and of the angle θ of the average moment of the probe region at the middle of the soft magnet (layers 35-44) is, in general, similar to that of the whole system, that is, via averaging over all Fe layers ('all').

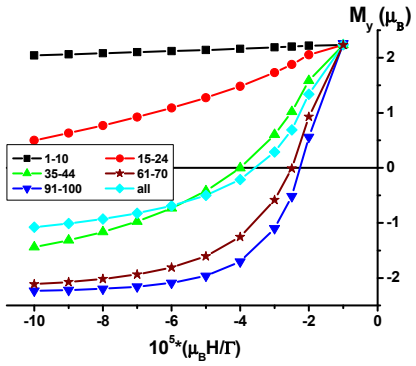
M_y (μ_B)
1-10
15-24
35-44
61-70
91-100
all
10^5*(μ_BH/Γ)

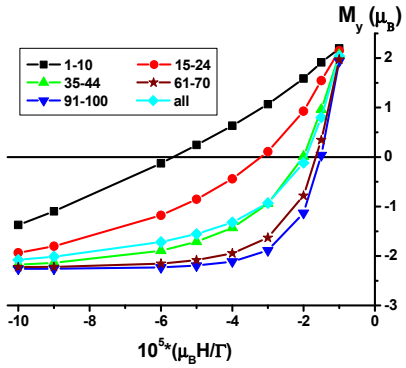
M_y (μ_B)
1-10
15-24
35-44
61-70
91-100
all
10^5*(μ_BH/Γ)

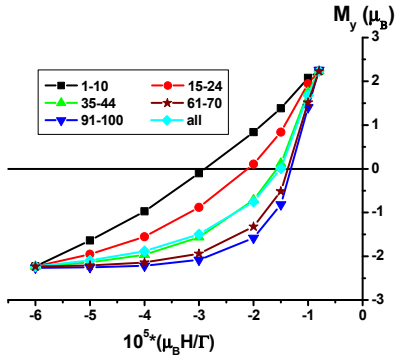
M_y (μ_B)
1-10
15-24
35-44
61-70
91-100
all
10^5*(μ_BH/Γ)

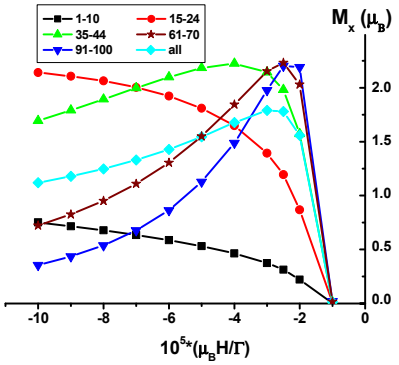
M_x (μ_B)
1-10
15-24
35-44
61-70
91-100
all
10^5*(μ_BH/Γ)

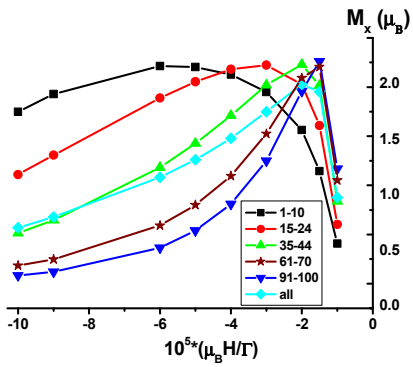
M_x (μ_B)
1-10
15-24
35-44
61-70
91-100
all
10^5*(μ_BH/Γ)

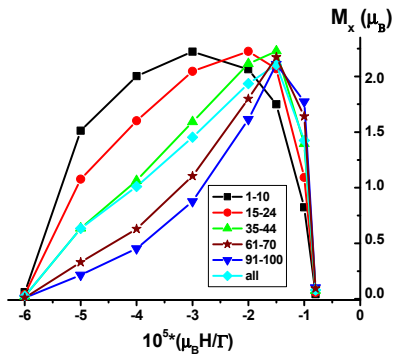
M_x (μ_B)
1-10
15-24
35-44
61-70
91-100
all
10^5*(μ_BH/Γ)

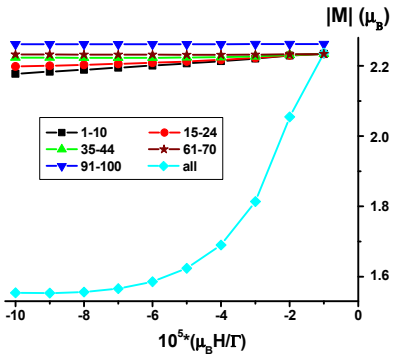
|M| (μ_B)
1-10
15-24
35-44
61-70
91-100
all
10^5*(μ_BH/Γ)

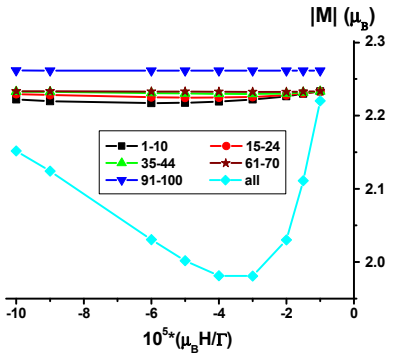
|M| (μ_B)
1-10
15-24
35-44
61-70
91-100
all
10^5*(μ_BH/Γ)

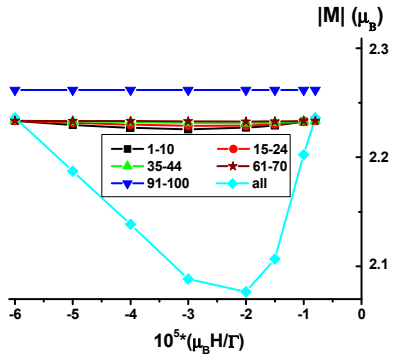
|M| (μ_B)
1-10
15-24
35-44
61-70
91-100
all
10^5*(μ_BH/Γ)

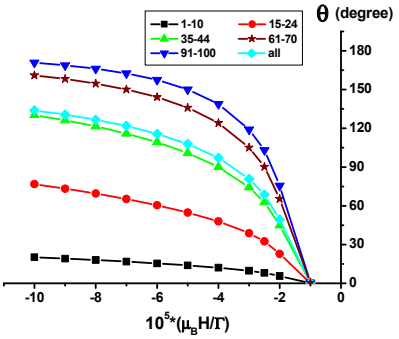
θ (degree)
1-10
15-24
35-44
61-70
91-100
all
10^5*(μ_BH/Γ)

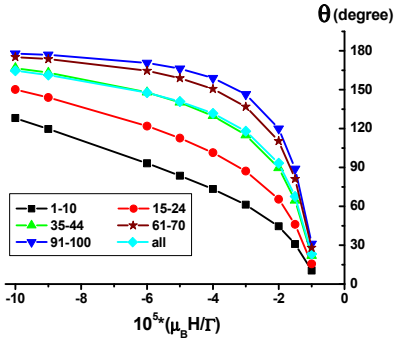
θ (degree)
1-10
15-24
35-44
61-70
91-100
all
10^5*(μ_BH/Γ)

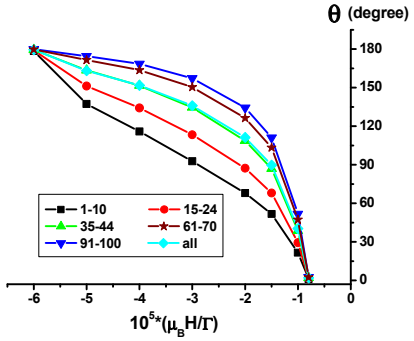
θ (degree)
1-10
15-24
35-44
61-70
91-100
all
10^5*(μ_BH/Γ)

Figure 6: From top to bottom: for different probe regions (10 ML thick) and for the whole Fe slab, we plot the longitudinal ($M_y$) and transverse ($M_x$) components of the average magnetic moment, its modulus (|M|) and the angle (θ) formed with the magnetization direction of the hard magnet, as a function of the applied magnetic field. Results are given for different values of the internal interfacial exchange field, as discussed in the text, to model the exchange coupling with the hard magnet: $\mu_B H_{\rm int} / \Gamma = \infty$ (left panel), $\mu_B H_{int} / \Gamma = 3 \cdot 10^{-3}$ (middle panel), and $\mu_B H_{int} / \Gamma = 2 \cdot 10^{-3}$ (right panel).

The knowledge of the modulus and direction of the local magnetic moments, in each layer, allows the calculation of the $R_{23}$ ratio for Mössbauer spectra, as explained in Sec. IV. In Fig. 7 (a) we plot the calculated layer-resolved $R_{23}$ ratio as a function of the applied magnetic field when considering the internal anisotropy field $H_{int}$ as infinite and assuming $^{57}$Fe atoms only in the probe layers and no $^{57}$Fe in the rest of the Fe slab. For probe layers at and close to the surface, and for the whole slab, the calculated $R_{23}$ values show non-monotonic behavior with a minimum, qualitatively similar to the corresponding experimental $R_{23}$ dependence (Fig. 5). However, for the interface layer, the calculated $R_{23}$ values drop almost linearly in Fig. 7 (a), contrary to the experimental case (sample A, Fig. 5). This disagreement can be connected with two factors. The first factor could be the distribution of $^{57}$Fe atoms inside the sample. The experimental probe layers contain 95% of $^{57}$Fe while the rest of the sample is made of natural Fe (which contains ~ 2% of $^{57}$Fe). The number of layers with natural iron is much larger than the number of probe layers, and their contributions in Mössbauer spectra (due to their 2% content of $^{57}$Fe) should be taken into account in the calculation. Moreover the signal from the interface can be weakened (as compared with the upper part) because conversion electrons from the interface have to travel through the whole Fe slab toward the surface. However, the latter effect, being small, is taken care of by Eqs. (4)- (6).

The calculated layer-resolved $R_{23}$ ratio for $H_{int} = \infty$, when taking into account the exact equivalent sample composition and distribution of $^{57}$Fe inside the Fe slab, are shown in Fig. 7 (b). One can notice that the general shape of the $R_{23}$ dependences now changes somewhat relative to that in Fig. 7 (a) and shows the tendency to move slightly toward the $R_{23}$ curve for the whole Fe slab ('all'). Such a tendency is also expected if the $^{57}$Fe probe layer would interdiffuse with the neighboring natural Fe layers. In Fig. 7 (b), the $R_{23}$ dependence of the interface (1-10 ML) and near-interface (15-24 ML) probe layers still exhibits a monotonic drop, but one can expect formation of a $R_{23}$ minimum even in the case of $H_{int} = \infty$ for severe $^{57}$Fe - $^{56}$Fe intermixing.

In Fig.7 (b), the general trends are still far apart from the experimental behavior (Fig. 5), in particular for the interface probe layers [1 – 10 ML in Fig. 7 (b)]. Therefore, a second correction factor must be considered, which is connected with the treatment of the exchange coupling at the

interface and the related effects of rotation of the interface Fe layer as a function of the external magnetic field, which is prevented so far since we assumed $H_{int} = \infty$. Now this constraint is released to perform a new set of calculations of the same system under the same conditions of probing with $^{57}$Fe. We have considered two different values of $H_{int}$ , namely $\mu_B H_{int}/\Gamma = 3 \times 10^{-3}$ and $2 \times 10^{-3}$. We note that although the value of this field $H_{int}$ largely exceeds the value of the applied external magnetic field H by one to two orders of magnitude, the moment of the interface Fe atoms is now able to rotate. Corresponding dependencies of the calculated layer-resolved $R_{23}$ ratio on the external field are shown in Fig. 7(c) for $\mu_B H_{int}/\Gamma = 3 \cdot 10^{-3}$ and in Fig. 7 (d) for $\mu_B H_{int}/\Gamma = 2 \cdot 10^{-3}$.

The important observation in Figs. 7 (c), (d) is the fact that all probe layers (including the interface layer) exhibit calculated $R_{23}$ dependences that are qualitatively similar to the corresponding experimental $R_{23}$ behavior (Fig. 5). In particular, the calculated $R_{min}$ values of all probe layers (including the interface layer) collapse at about the same value of $R_{min} = 0.8 \pm 0.1$ (for $h_{int} = 3 \times 10^{-3}$, Fig. 7 (c) ) and of $R_{min} = 0.7 \pm 0.1$ (for $h_{int} = 2 \times 10^{-3}$, Fig. 7 (d) ). Comparison of Fig.6 (bottom panels) with Figs. 7 reveals that the calculated minima, $R_{min}$, appear at $\theta = 90°$, *i.e.*, when the approximately homogeneous probe-layer magnetization is oriented along the x axis (or parallel to the in-plane projection of the incoming Mössbauer $\gamma$-ray). In the ideally unidirectional (collinear) case, this would yield the limiting value of $R_{min} = 0.57$ (for our geometry with $\Phi = 30°$). Our calculated $R_{min}$ values are all close to or only slightly higher than this limiting value. The observed experimental $R_{min}$ ratios of all samples also collapse at a common (though higher) value of 1.2(1), except for the interface probe layer (sample A) which shows an even higher ratio of $R_{min} = 1.7(1)$. The reason for the generally higher experimental $R_{min}$ values as compared to the calculated ones cannot be interdiffusion of probe-layer $^{57}$Fe and natural Fe alone, since the theo retical upper limit of $R_{min}$ in this case is equal to $R_{min}$ for the whole Fe slab ('all'), which is equal to 0.8 – 0.9 according to Fig. 7 (c), (d). Therefore, the reason for the quantitative discrepancy between calculated and experimental $R_{min}$ values must be related to factors so far not taken into account by our theory. Such a factor could be the existence of a distribution of exchange anisotropy fields $h_{int}$ at the interface instead of a single field. Then, minima, $R_{min}$, of $R_{23}$ for different $h_{int}$ values will be achieved at different external fields $h_{min}$. As an example for the effect of a simple $h_{int}$ distribution on $R_{23}$, we have calculated the average $R_{23}$ ratio, $\langle R_{23} \rangle(h)$, for a particular probe layer from the average quantity $\langle \cos^2\Psi \rangle_{av}$, using Eq.(2). $\langle \cos^2\Psi \rangle_{av}(h)$ was calculated for a particular probe layer from the relation $\langle \cos^2\Psi \rangle_{av}(h) = [\langle \cos^2\Psi \rangle(h_{int}=\infty) + \langle \cos^2\Psi \rangle(h_{int}=3x10^{-3}) + \langle \cos^2\Psi \rangle(h_{int}=2x10^{-3})]/3$, where the three $\langle \cos^2\Psi \rangle$ terms in the rectangular brackets correspond to the cases of Figs. 7 (b), (c) and (d), respectively. Thus, this $h_{int}$ distribution contains the three contributions at $h_{int} = \infty$, $3x10^{-3}$ and $2x10^{-3}$ with equal weight. The result, as shown in Fig. 7 (e), gives a much better agreement with the experimental $R_{23}(H)$ behavior (Fig. 5) than each

of the $R_{23}(h)$ dependences calculated with a single exchange anisotropy field $h_{int}$. In particular, the calculated minimum for the interface layer (1 - 10 ML) is now at $<R_{23}>_{min} = 1.6$, and in the experiment it is at $R_{min} = 1.7$. The calculated minima $<R_{23}>_{min}$ for the other probe layers lie in the range of 1.0 – 1.3 as compared to the experimental $R_{min}$ range of 1.15 – 1.2. Moreover, the general shape of the corresponding curves is similar in theory [Fig. 7 (e)] and experiment (Fig. 5). Considering a distribution of interface couplings, $h_{int}$, a surprising feature of the experimental $R_{23}$ – *vs.* – H data (Fig. 5) finds a natural explanation. In Fig. 5, for the whole range of magnetic fields, $R_{23}$ of sample B was found to be lower than $R_{23}$ for sample A (interface). Therefore, even in large magnetic fields close to the field of irreversible demagnetization, $H_{irr}$, of the hard magnet, the Fe magnetic moments separated by 4 nm from the interface prove to be less aligned along the external field than the very interface Fe moments. Taking a distribution of $h_{int}$ into account, we obtain exactly such a behavior in the theory: In both Figure 7 (e) (theory) and Figure 5 (experiment) the red full circles lie below the black full squares in the whole range of magnetic fields. Our result provides evidence for the existence of a broad distribution of exchange fields, $h_{int}$, at the real (Co-Sm)/Fe interface. The origin of this $h_{int}$ distribution could be related to the fact that strong Co/Fe interdiffusion occurs at the interface, leading to an interfacial Fe-Co alloy, as proven by our CEMS results. The formation of the Fe-Co alloy likely occurs inhomogeneously across the hard/soft interface, considering the polycrystalline nature of the *bcc*-Fe layer. This will lead to local fluctuations of the exchange coupling $h_{int}$ at the hard/soft interface. Fluctuations in the interface coupling were conceived earlier in order to interpret the observed strongly reduced domain nucleation field at irreversible switching of SmFe/NiFe hard/soft bilayers as compared to the nucleation field of a single SmFe film [19]. Our present findings support such an interpretation.

Note that the (irreversible) nucleation of reversed domains in the hard magnet may possibly start even at relatively low applied-field magnitudes via the so-called magnetic after-effect due to the long measurement time for taking a Mössbauer spectrum (~ 24 h). The existence of reversed domains leads to an increase of the $R_{23}$ ratio, since the angle $\Psi$ in Eq. (2) is 90° for these switched domains. However, such a $R_{23}$ enhancement should be observed for all samples A to E. In the experiment, however, only $R_{23}$ for sample A (probe layer at the interface) is found to be much higher than for all the other samples B to E (Fig. 5). Therefore, the nucleation and propagation of reversed domains at low fields, corresponding to the reversible part of the hysteresis loops (Fig. 2), does not play an essential role in the formation of the $R_{23}(H)$ behavior. Even for such a high field value as $|\mu_0 H| = 450$ mT, where $R_{23}(H)$ has its minimum value $R_{min}$ for sample A, $R_{23}(H)$ for sample B (with its $^{57}$Fe probe layer next-nearest to the hard/soft interface) increases only very slightly relative to its $R_{min}$ value (Fig. 5).This demonstrates that even at $\mu_0 H = -450$ mT reversed domains play only a negligible role, and the minimum in $R_{23}(H)$ of sample A (interface) is not substantially determined by nucleation and

propagation of reversed domains. Instead, our present calculations provide strong evidence for the reason why $R_{min}$ of sample A is higher than $R_{min}$ of the other samples B to E: the $^{57}Fe$ probe layer in sample A senses directly the proposed wide distribution of exchange-anisotropy fields $H_{int}$ (or $h_{int}$) at the hard/soft interface.

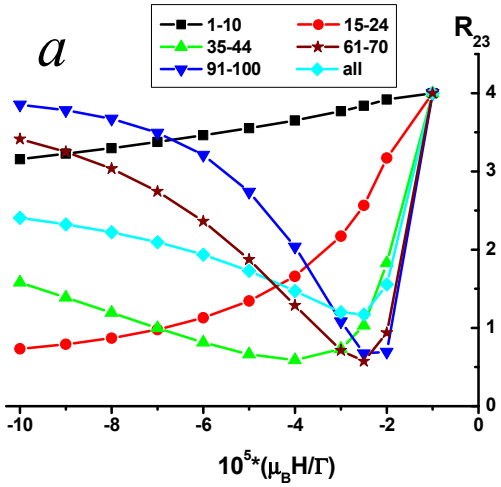
a
1-10
15-24
35-44
61-70
91-100
all
R23
10^5*(μBH/Γ)

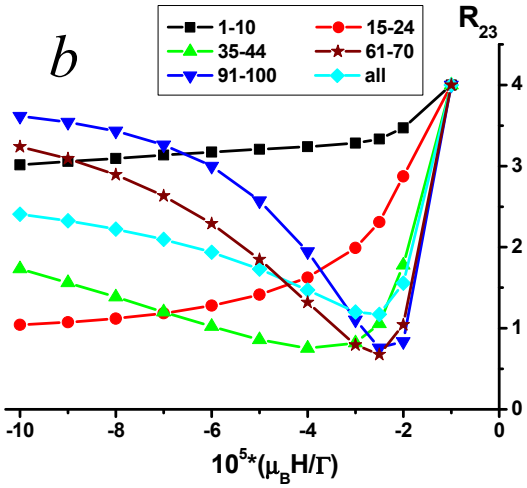
b
1-10
15-24
35-44
61-70
91-100
all
R23
10^5*(μBH/Γ)

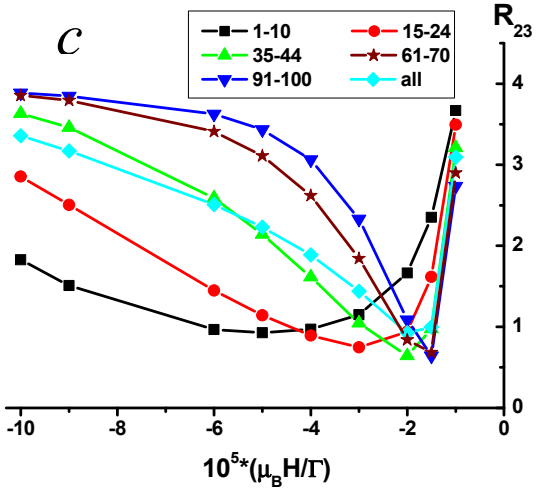
c
1-10
15-24
35-44
61-70
91-100
all
R23
10^5*(μBH/Γ)

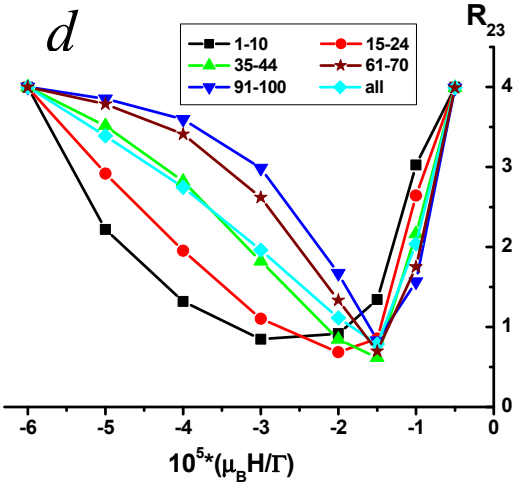
d
1-10
15-24
35-44
61-70
91-100
all
R23
10^5*(μBH/Γ)

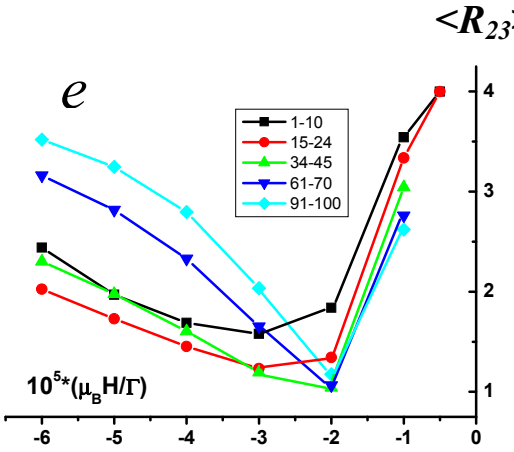
<R23>
e
1-10
15-24
34-45
61-70
91-100
10^5*(μBH/Γ)

Figure 7: Calculated $R_{23}$ ratio versus normalized external field $h = \mu_B H/\Gamma$ for 10-ML thick $^{57}$Fe probe layers placed in different probe regions within the 100-ML thick Fe slab: 1-10 ML (interface, black full squares), 15 – 24 ML (red full circles), 35 – 44 ML (green full triangles tip up), and 91 – 100 ML (surface, blue full triangles tip down). The case of a homogeneous 100-ML thick $^{57}$Fe slab is also shown (turquoise full diamonds). Special cases are considered: (a) the internal interfacial exchange field $H_{int} = \infty$, $^{57}$Fe atoms are only in the probe layer, no $^{57}$Fe in the rest of the Fe slab; (b) $H_{int} = \infty$, 95 % $^{57}$Fe in the probe layers and ~ 2 % $^{57}$Fe in the (natural) Fe slab, equivalent to the nominal experimental sample composition; (c) as in case (b), but taking $h_{int} = \mu_B H_{int}/\Gamma = 3\text{x}10^{-3}$; (d) as in case (b), but taking $h_{int} = \mu_B H_{int}/\Gamma = 2\text{x}10^{-3}$. (e): Calculated average ratio $<R_{23}>$ as described in the text (The lines are guides for the eye).

We note that the irreversible switching of the magnetization of the hard magnet in the exchange spring should start slightly before, at or slightly after the angle formed by the interfacial Fe magnetic moments reaches 90 degrees, counted from the hard-magnet anisotropy axis. Indeed, it was experimentally shown that for thin soft magnetic slabs, the magnetizations of the hard and the soft phases rotate simultaneously, whereas for thicker Fe slabs, a spin spiral can be formed [22]. For the latter case, lower external fields for switching are required for thicker Fe slabs. Similar effects were found by phenomenological theories [19,22,23,32,34,35[. Our results indicate that, despite the huge internal interfacial exchange-anisotropy field $H_{int}$ of the order of tens of Tesla, the formation of the spin spiral in our 100 ML Fe slab for applied external fields of less than 1 T gives rise to a rotation of the interfacial Fe moment, which could not take place if the soft phase is formed by very few Fe layers. This rotation at the interface is due to the local ferromagnetic exchange couplings existing within the Fe slab.

To understand such a behavior, let us consider a simple mechanical model representing a system of weights vertically connected by weightless springs, suspended in a uniform gravitational field. Obviously, the deformation of the springs, and hence the force of elasticity associated with this deformation, will increase towards the point of suspension. The deformation of the first spring (counted from the point of suspension) will be determined by the total weight of the entire system. Similar behavior is observed in the exchange spring system in an external magnetic field. Rotation of the magnetic moments relative to the moments of neighboring atomic layers in the soft phase increases towards the interface with the hard phase, together with an effective magnetic force from the underlying layers. Therefore, the model for the spin structure in the soft phase, which assumes a linear increase of the rotation angle with distance from the soft/hard interface, can be used only as a rough approximation. Furthermore, neglecting the influence of upper soft layers on the

magnetic behavior of probe layers can lead to a wrong conclusion about the magnetic behavior of the hard phase.

Irreversible switching of the hard-layer magnetization will take place most probably in an external field which is lower than the one that leads to a rotation of more than 90° of the bottom (interfacial) Fe-layer magnetic moment. As a result, the minimum value, $R_{min}$, of the $R_{23}$ ratio measured experimentally (Fig. 5) is larger than the one calculated for $\mu_B H_{int}/\Gamma = (2 - 3) \times 10^{-3}$, but is smaller than the calculated $R_{23}(H)$ values of the interface layers computed for $\mu_B H_{int}/\Gamma = \infty$ [Fig. 7(a),(b)]. (Note that for the latter case $R_{min}$ is never reached within the range of $\mu_B H/\Gamma$ values of the calculations). The value of the external field, $H_{min}$, corresponding to the minimum ($R_{min}$) of $R_{23}$ for the interface probe layers, provides an estimation for the external field at which the irreversible magnetisation reversal of the hard phase starts. Experimentally, this occurs at $\mu_0 H_{min} = -450$ mT for sample A, which is equivalent to $\mu_B H_{min}/\Gamma = -2.6 \times 10^{-5}$ if we assume a value of 0.1 eV for $\Gamma$.

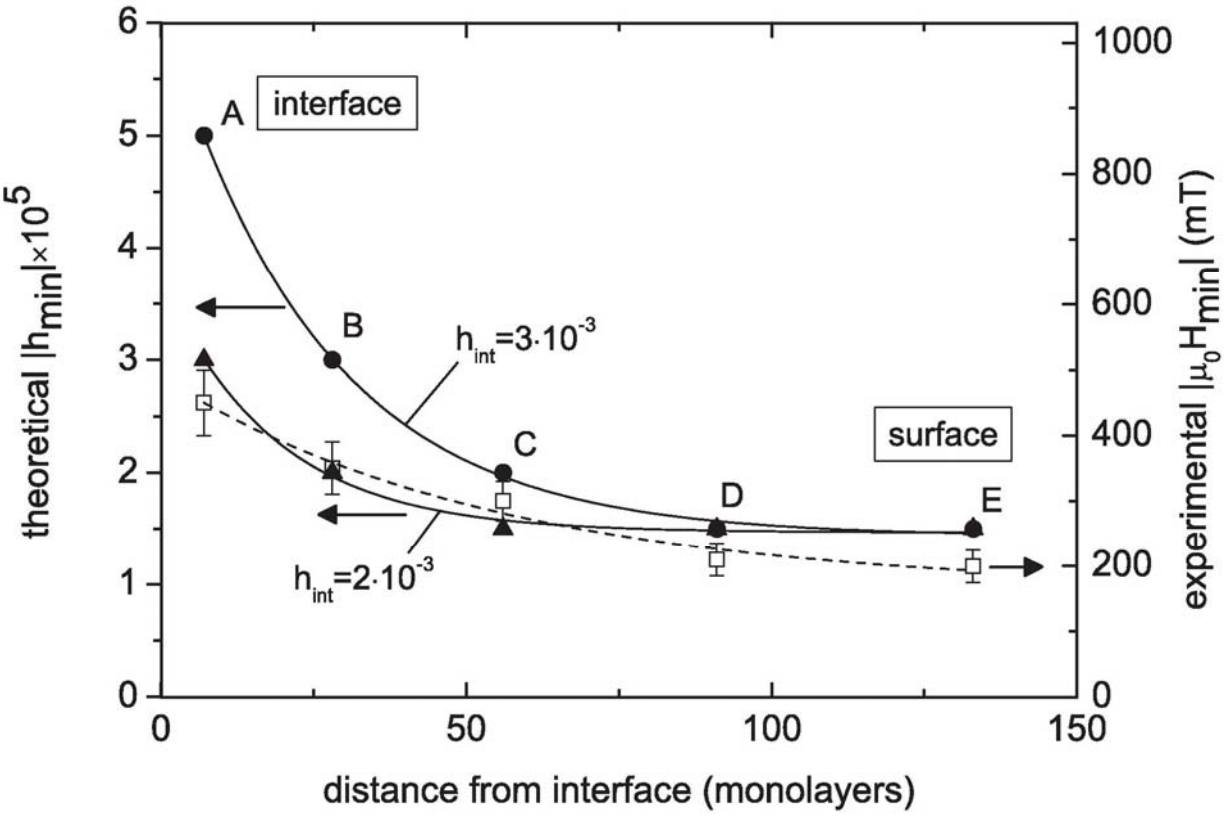


Figure 8: Theoretical field $|h_{min}|$ (left scale) for $h_{int} = 3 \times 10^{-3}$ and $2 \times 10^{-3}$, respectively, and experimental field $|\mu_0 H_{min}|$ (right scale) as a function of the experimental $^{57}$Fe probe-layer distance from the Sm-Co/Fe interface for samples A – E. (The lines are guides for the eye).

Figure 8 displays the theoretical $|h_{min}|$ values (left scale) and the experimental $|\mu_0 H_{min}|$ values (right scale) as a function of the average $^{57}$Fe probe-layer distance from the interface for the different samples. Here, the theoretical distance was scaled to the average experimental distance by a factor of 1.4. The unit of the left vertical scale corresponds to 173 mT on the right vertical scale that was calculated using $\Gamma = 0.1$ eV. $|\mu_0 H_{min}|$ can be seen to drop continuously with increasing distance for samples A – D. As to $|h_{min}|$, it drops relatively fast with distance for $h_{int} = 3 \times 10^{-3}$ (stronger interface coupling), while the decrease is slower for $h_{int} = 2 \times 10^{-3}$ (weaker interface coupling). The theoretical dependence seems to saturate for samples D and E, which include probe layers close to or at the surface. We like to mention that Fig. 8 provides only a qualitative comparison between calculation and experiment, since the distance from the interface was scaled and the d-level width $\Gamma$ is known only approximately for the theoretical data.

In Figure 9 we display the calculated in-plane Fe-spin rotation angle $\theta$ (obtained from Fig. 6, bottom panels) as a function of the $^{57}$Fe probe-layer distance z from the Sm-Co/Fe interface with the applied field h as a parameter. The interface exchange field $h_{int}$ is larger ($3 \times 10^{-3}$) in Fig. 9 (a) and smaller ($2 \times 10^{-3}$) in Fig. 9 (b). Figure 9 demonstrates that the $\theta$ - *vs.* - z dependence in the Fe slab is strongly nonlinear. The dependences for smaller $|h_{int}|$ [Fig. 9 (b)] appears to be flatter than those for larger $|h_{int}|$ [Fig. 9 (a)]. The positive slope $d\theta/dz$ decreases almost linearly from the interface towards the surface (not shown). This means that when moving from the interface to the surface $\theta$ changes more and more slowly. Figure 9 strongly suggests that a linear $\theta$ – *vs.* - z relationship (or a uniform spin-spiral model) [11,12] provides only an approximate description of the real spin structure in the Fe slab.

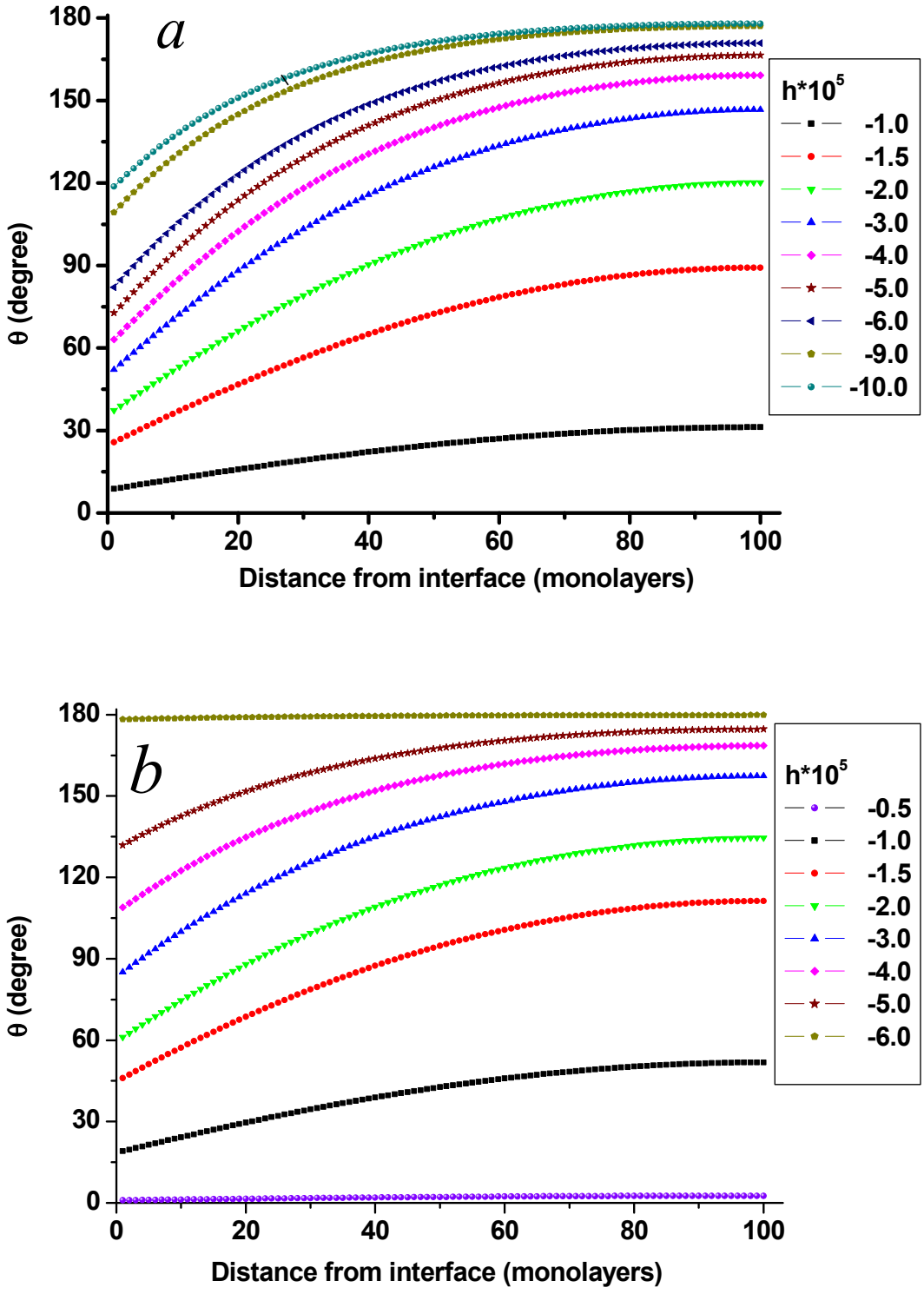


Figure 9: Calculated in-plane Fe-spin rotation angle θ versus the $^{57}$Fe probe-layer distance from the Sm-Co/Fe interface for different applied-field values h: (a) for $h_{int} = 3 \times 10^{-3}$, (b) for $h_{int} = 2 \times 10^{-3}$

## VI. CONCLUSIONS

We have studied the in-plane magnetization reversal process in nanoscale (Sm-Co)/Fe bilayer exchange-spring magnets with in-plane uniaxial magnetic anisotropy by magnetometry, $^{57}$Fe Mössbauer spectroscopy (CEMS) and quantum-mechanical Fe-spin structure calculations. Magnetization loops along the easy direction exhibit properties typical of exchange spring magnets. Mössbauer spectroscopy at inclined γ-ray incidence on thin $^{57}$Fe probe layers gives depth-selective (atomistic) information (via the line intensity ratio $R_{23}$) about the in-plane rotation of Fe magnetic moments during magnetization reversal. The applied-field dependence of $R_{23}$ was found to be depth-dependent and non-monotonic, providing proof of Fe spin rotation.

The measured $R_{23}$-*vs.*-H dependence is characterized by a depth-dependent minimum at ($H_{min}$, $R_{min}$), where Fe magnetic moments roughly adopt an average perpendicular orientation during their reversal from positive to negative easy axis orientation. With decreasing field, surface and near-surface Fe moments reverse their direction already before the (macroscopic) coercive field, $H_C$, is reached, whereas Fe moments near the (Sm-Co)/Fe interface reverse their direction only for fields stronger than $H_C$. A monotonic decrease of $H_{min}$ with increasing distance from the hard/soft interface is observed. Our experimental findings are qualitatively consistent with the formation of an Fe spin spiral structure upon reversal. Rotation of Fe magnetic moments takes place even in the interface region in applied fields far below the field of irreversible switching, $H_{irr}$, of the hard phase. Further, formation of a Fe-Co alloy is observed in the hard/soft interface region.

For comparison with the experimental results, we have determined the non-collinear Fe spin structure, the magnetic moment distribution and the resulting Mössbauer $R_{23}$ ratio during magnetization reversal through electronic structure calculations on the basis of a microscopic (quantum-mechanical) Hamiltonian for itinerant electrons. A tuning parameter is the (normalized) uniaxial internal exchange-anisotrpy field, $h_{int}$, at the hard/soft interface. Our calculated $R_{23}$ ratios for probe layers in different depths of the soft Fe layer exhibit similar features as observed in the experiment, in particular a minimum in the field-dependence of $R_{23}$. In the calculation, the Fe magnetic moments form an angle of $\theta = 90°$ (relative to the easy axis direction) at the $R_{23}$ minimum, indicating switching from positive to negative direction at $h_{min}$. $R_{min}$ is found to increase with the interface coupling $h_{int}$, and, thus, can be used as a measure of $h_{int}$. Evidence is given for the existence of a distribution of exchange fields, $h_{int}$, accounting for the coupling strengths at the hard/soft interface. This local variation of $h_{int}$ exists within each sample, but not across our different samples. Since the average values of $h_{int}$ for each of the samples are quite similar (as evidenced by their similar values of $H_{ex}$ in the magnetization loops), the

observed spread of $H_{irr}$ values across the different samples does not reflect the distribution of $h_{int}$ values within each sample. The calculations also show that there is no linear relationship between the Fe-spin rotation angle θ and the probe-layer depth z. In probe layers close to the interface with the hard magnet, the relative rotation of Fe magnetic moments in neighboring magnetic layers is larger than in upper layers farther away from the interface. However, the assumption of a collinear (unidirectional) Fe spin structure within a thin (10 ML) probe layer is approximately justified.

Our work demonstrates that Mössbauer spectroscopy with thin $^{57}$Fe probe layers is a unique method to provide microscopic depth-selective information on the magnetization reversal process in exchange-spring magnets. The simulation of the magnetic structure in an external field on the basis of a microscopic (quantum-mechanical) Hamiltonian for itinerant electrons can be used to prove the intuitive physical considerations used for the interpretation of experimental results. Moreover, it can lead to a new view on the underlying physics and also may lead to the revision of assumptions considered earlier.

## ACKNOWLEDGMENTS

The expert technical assistance of U. von Hörsten (Duisburg-Essen) is gratefully acknowledged. W.K. appreciates stimulating discussions with J. Kirschner (Halle). This work was partially supported by DFG-RFBR cooperative Grant No. 10-02-91330, and by the Deutsche Forschungsgemeinschaft ( SFB 491 Bochum/Duisburg) by the Spanish Ministry of Science and Innovation in conjunction with the European Regional Development Fund (project FIS2008-02490/FIS), and by Junta de Castilla y León (project GR120). V.M.U. acknowledges the financial support and the kind hospitality from the University of Valladolid (Spain). V.K. acknowledges financial support by the Alexander-von-Humboldt Foundation and PNII-71-032. Work at Argonne was supported by U. S. DOE Office of Science under Contract No. DE-AC02-06CH11357.

[a] permanent address: JSC "SSC RIAR", Dimitrovgrad, 433510, Russia

## REFERENCES

1. S. S. P. Parkin, M. Hayashi, and L. Thomas, Science **320**, 190 (2008).

2. F. Nolting, A. Scholl, J. Stöhr, J. W. Seo, J. Fompeyrine, H. Siegwart, J.-P. Locquet, S. Anders, J. Lüning, E. E. Fullerton, M. F. Toney, M. R. Scheinfein, and H. A. Padmore, Nature **405**, 767 (2000).

3. C. H. Marrows and B. C. Dalton, Phys. Rev. Lett. **92**, 097206 (2004).

4. S. D. Bader, Rev. Mod. Phys. **78**, 1 (2006).

5. K.V. O'Donovan, J. A. Borchers, C. F. Majkrzak, O. Hellwig, and E. E. Fullerton, Phys. Rev. Lett. **88**, 067201 (2002).

6. R. Röhlsberger, H. Thomas, K. Schlage, E. Burkel, O. Leupold, and R. Rüffer, Phys. Rev. Lett. **89**, 237201 (2002).

7. T. Klein, R. Röhlsberger, O. Crisan, K. Schlage, and E. Burkel, Thin Solid Films **515**, 2531 (2006).

8. W. A. A. Macedo, B. Sahoo, J. Eisenmenger, M. D. Martins, W. Keune, V. Kuncser, R. Röhlsberger, O. Leupold, R. Rüffer, J. Noguès, Kai Liu, K. Schlage, and Ivan K. Schuller, Phys. Rev. B **78**, 224401 (2008).

9. J. S. Jiang, S. D. Bader, H. Kaper, G. K. Leaf, R. D. Shull, A. J. Shapiro, V. S. Gornakov, V. I. Nikitenko, C. L. Platt, A. E. Berkowitz, S. David and E. E. Fullerton, J. Phys. D: Appl. Phys. **35**, 2339 (2002).

10. O. Hellwig, J. B. Kortright, K. Takano, and E. E. Fullerton, Phys. Rev. B **62,** 11694 (2000).

11. V. E. Kuncser, M. Doi, W. Keune, M. Askin, H. Spies, J. S. Jiang, A. Inomata, and S. D. Bader, Phys. Rev. B **68,** 064416 (2003).

12. W. Keune, V. E. Kuncser, M. Doi, M. Askin, H. Spies, B. Sahoo, E. Duman, M. Acet, J. S. Jiang, A. Inomata and S. D. Bader, J. Phys. D: Appl. Phys. **35**, 2352 (2002).

13. V. M. Uzdin and W. Keune, J. Phys.: Condens. Matter. **19**, 136201 (2007).

14. V. M. Uzdin and A. Vega, Nanotechnology **19**, 315401 (2008).

15. V.M. Uzdin, A. Vega, Phys. Rev. B **77**, 134446 (2008).

16. E. E. Fullerton, J. S. Jiang, and S. D. Bader, J. Magn. Magn. Mater. **200**, 392 (1999).

17. Y. Choi, J. S. Jiang, Y. Ding, R. A. Rosenberg, J. E. Pearson, S. D. Bader, A. Zambano, M. Murakami, I. Takeuchi, Z. L. Wang, and J. P. Liu, Phys. Rev. B **75**, 104432 (2007).

18. R. A. Brand, Nucl. Instrum. Methods Phys. Res. **28**, 417 (1987).

19. D. Chumakov, R. Schäfer, D. Elefant, D. Eckert, L. Schultz, S. S. Yan, and J. A. Barnard, Phys. Rev. B **66**, 134409 (2002).

20. V. Kuncser, W. Keune, M. Vopsaroiu, and P. R. Bissell, Nucl. Instrum. Methods Phys. Res. B **245**, 539 (2006).

20 W. A. A. Macedo, B. Sahoo, V. Kuncser, J. Eisenmenger, I. Felner, J. Noguès, Kai Liu, W. Keune, and Ivan K. Schuller, Phys. Rev. B **70**, 224414 (2004).

22. E. E. Fullerton, J. S. Jiang, M. Grimsditch, C. H. Sowers, and S. D. Bader, Phys. Rev. B **58**, 12193 (1998).

23. K. Mibu, T. Nagahama, and T. Shinjo, J. Magn. Magn. Mater. **163**, 75 (1996).

23. D. Chumakov, R. Schäfer, D. Elefant, D. Eckert, L. Schultz, S. S. Yan, and J. A. Barnard, Phys. Rev. B **66**, 134409 (2002).

24. S. Sawatzki, R. Heller, Ch. Mickel, M. Seifert, L. Schultz, and V. Neu, J.Appl. Phys. **109**, 123922 (2011).

25. R. S. Preston, S. S. Hanna, and J. Heberle, Phys. Rev. **128**, 2207 (1962).

26. P. J. Schurer, Z. Celinski, and B. Heinrich, Phys. Rev. B **48**, 2577 (1993); **51**, 2506 (1995).

27. C. E. Johnson, M. S. Ridout, T. E. Cranshaw, and P. E. Madsen, Phys. Rev. Lett. **6**, 450 (1961).

28. S. Chikazumi, *Physics of Magnetism* (John Wiley and Sons, New York, 1964) p. 73

29. V. M. Uzdin and L. Häggström, Phys. Rev. B **72**, 024407 (2005).

30. J. S. Jiang, J. E. Pearson, Z. Y. Liu, B. Kabius, S. Trasobares, D. J. Miller, and S. D. Bader, J. Appl. Phys. **97**, 10K311 (2005).

31. D. Wu, Q. Zhang, J.P. Liu, R.F. Sabirianov, J. Nanoscience and Nanotechnology **8**, 3036 (2008).

32. G. Asti, M. Solzi, M. Ghidini, F.M. Neri, Phys. Rev. B 69, 174401 (2004).

33. D. Liljequist, T. Ekdahl, and U. Bäverstam, Nucl. Instrum. Methods **155**, 529 (1978).

34. R. Pellicelli, M. Solzi, V. Neu, K. Häfner, C. Pernechele, and M. Ghidini, Phys. Rev. B **81**, 184430 (2010).

35. E. Goto, N. Hayashi, T. Miyashita, and K. Nakagawa, J. Appl. Phys. **36**, 2951 (1965).